# Deformation Behaviour of C-Mn440 Automobile Steel under Varying Strain Rates

Thesis submitted in partial fulfilment of the requirements for the award of the degree of

**Master of Technology**

in

**Mechanical Engineering**

**[**Specialization**:** Steel Technology]


Submitted by

**AWANISH KUMAR MISHRA**

Roll No.-**212MM2420**

Department of Metallurgical and Materials Engineering

National Institute of Technology

Rourkela-769008

**May 2014**

# Deformation Behaviour of C-Mn440 Automobile Steel under Varying Strain Rates

Thesis submitted in partial fulfilment of the requirements for the award of the degree of

**Master of Technology**

in

**Mechanical Engineering**

**[**Specialization**:** Steel Technology]


Submitted by

**AWANISH KUMAR MISHRA**

Roll No.-**212MM2420**

Under the Guid**a**nce of

**Prof. KRISHNA DUTTA**

Metallurgical & Materials Engineering Department
National Institute of Technology Rourkela
Rourkela -769008

**Dr. ARPAN DAS (Scientist)**

Materials Science & Technology Division
National Metallurgical Laboratory
Jamshedpur- 8

**National Institute of Technology Rourkela**

## C E R T I F I C A T E

This is to certify that the thesis entitled, "**DEFORMATION BEHAVIOUR OF C-Mn440 AUTOMOBILE STEELUNDER VARYING STRAIN RATES**" submitted by **Mr. AWANISH KUMAR MISHRA** in partial fulfilment of the requirements for the award of Master of Technology Degree in **MECHANICAL ENGINEERING** with specialization in "**STEEL TECHNOLOGY**" at the National Institute of Technology, Rourkela is authentic work carried out by him under our supervision and guidance.

To the best of our knowledge, the matter embodied in the thesis has not been submitted to any other University/Institute for the award of any Degree or Diploma.


**Prof. KRISHNA DUTTA**
Dept. of Metallurgical and Materials Engg.
National Institute of Technology
Rourkela 769 008

Date:
Place:

**Dr. ARPAN DAS (Scientist)**
Materials Science and Technology Division
CSIR - National Metallurgical Laboratory
Jamshedpur 831 007

Date:
Place:

# Acknowledgements

I avail this opportunity to express my heartfelt gratitude and regards to all those who helped me a lot throughout my M. Tech course. First of all, I would like to convey my deep regards and thanks to my guide **Prof. Krishna Dutta,** Department of Metallurgical & Materials Engineering, National Institute of Technology, Rourkela who always helped me as friend and elder brother without his invaluable guidance, untiring efforts and meticulous attention at all stages during my project work I cannot complete my work.

I would also like to convey my deep regards to my co-supervisor **Dr. Arpan Das, Scientist,** National Metallurgical Laboratory, Jamshedpur, for his indebted help and valuable suggestions for the accomplishment of my experimentation and dissertation work.

I would also like to thank **Prof. B. B. Verma** who always motivated me and enlighten me with his valuable suggestions. I am grateful to **Dr. S. Tarafdar (Chief scientist & head)**, **Dr. N. Parida (Chief scientist & head)**,**Dr. S. Sivaprasad (Principal scientist), Dr. J. K. Sahu (Principal scientist), and Dr. H N Bar(Scientist)**National Metallurgical Laboratory, and Jamshedpur who gave me suggestion on experimental work, carrier and general behavior. They also taught me about valuable managerial skills to manage a project.

I am greatly indebted to the **Dr. S. Srikanth** Director, NML Jamshedpur, who allowed me to work at NML for the maximum part of my experiments. By this, I got the opportunity to be a part of a premiere research organization like NML Jamshedpur. Also, the wonderful testing and working facilities along with a friendly work culture in NML Jamshedpur has constantly motivated me to carry out my work in a decent pace.

I also like to thank, all my group members of Mechanical property evaluation of MST Division in NML Jamshedpur, wherefrom I have got all sorts of help whenever needed, especially from Mr. Anindya Das, Mr. Kaustav Barat, Mr. K. Priya Ajit and Mr. Chandan Kumar Sharma, and many more.

Many a times in my life I have come across and felt the true virtue of the phrase'A friend in need is a friend in deed'. I have been honestly endeavored with friends who have made me feel like that. Here comes the opportunity to thank all my colleagues in N.I.T Rourkela (Mr.Dipesh mishra, Mr. Prem prakash seth, Mr. Amit jashwal , Mr.Abhisek tripathi , Mr. Pawan sahoo, Md. Afzal Hussain,) my batchmates in N.I.T. Rourkela.

Lastly but not the least, no work could have been conducted without the support of my parents and my family. They supported my endeavor for knowledge from childhood and my passion for learning owes to their encouragement.

**Awanish Kumar Mishra**

# Declaration

I certify that

The work contained regarding to my experimental analysis is totally original and I have been done all experimental work under the supervision of my supervisors. This work does not submitted anywhere for getting any degree and diploma.

During completing the thesis work, I have followed rule and regulation of my institute and also mentioned the reference from where I have use the data from my thesis work.

Signature of the Student

# Contents

# Abstract

The prime objective of vehicle designers is to produce vehicles with fuel-economy along with the safety standards imposed by the government and stringent consumer demands. It is known that reducing the weight of a vehicle is a straight forward strategy to improve fuel-economy, but it can potentially create safety problems which in turn leads to increased utilization of high strength steel sheets for the automobile body components. *C-Mn* and *DP* steels consist of outstanding combination of both strength and ductility. High strain rate experiments are generally used to study the material behaviour when these are subjected to high speed impacts, like crash. The mechanical behaviour of these materials at high strain rates is considerably different from that observed at quasi-static loading because of the strain rate sensitivity of the material. Hence, automotive industries are continuously engaged with designing newer materials for car body applications.

In this investigation, many quasi static tensile experiments were carried out at various strain rates on C-Mn 440 steel at ambient temperature. It has been observed that yield and tensile strengths of the material increase drastically while %EL and %RA significantly decrease with the strain rate. The fracture surface reveals dimple morphology with variation of dimple geometry with strain rate; average dimple diameter increases and dimple density decreases with strain rate. The void accumulation (i.e., void density) inside the material increases with the increase in true strain for all the strain rates. At the initial stage of strain, void density increases slowly and at the later stage, void density increases rapidly. The dislocation densities in all deformed specimens have been calculated from X-ray diffraction profile analyses using modified Williamson-Hall method; the results show that dislocation density increases with strain rate.

**Keywords**: C-Mn440 steel, strain rate, tensile test, void density, dislocation density

# List of Figures

# List of Tables

# CHAPTER .1

# Introduction

## 1.1 Introduction:

Recent high requirement for vehicle lightening in the automobile sector requirement flat carbon steel manufacturers to develop advanced newer grades of materials which are capable of fulfilling the gradually more stringent technical demand of market. For this, the steel industries /automobile industries are regularly trying to produce newer kinds of steels with superior properties. C-Mn steel is one of such kind which is having high strength, high elongation, high hardness and toughness. Carbon steel can be produced at a minimum cost by applying with carbon and manganese. Separately from the positive economic impact, the superior mechanical properties were obtained by applying these two elements. [2]. As can be expected, in such applications the car body may face crash, high impact and various kinds of states of stresses. One of these could be manifested experimentally as 'loading at different rates of straining'. It is well known that materials' behaviours under different strain rates vary [1].Although scattered results may be available for the effect of strain rate on mechanical behavior of the steel, understanding about their response in dynamic loading conditions is limited. Therefore the aim of this investigation is to study the deformation behaviour of C-Mn440 steel at different strain rates. The test matrix has been chosen in such a manner that it can reflect the actual loading conditions during their utilization. This kind of steel is usually ductile in nature [2]. Further, it is known that the micromechanism of ductile fracture involves the initiation, growth and coalescence of microvoids [3]. Includes initiation of Voids from flowing factor like precipitates, second phase particles, inclusions etc, in the metallic matrix and grow under the influence of manly two factor like plastic strain and hydrostatic stress [3,4]. However, it would be interesting as well as of scientific importance to know the void formation characteristics at different true strain levels of a specimen during tensile loading. Therefore these features have been studied rigorously at various levels of true strains under the investigated strain rates. In the present investigation, attempts have been made to

study the effect of strain rate on the tensile behaviour of C-Mn440 steel, its role in void formation on tensile straining at strain rates ranging between 0.0001 and 0.1 $s^{-1}$, and quantitatively correlate fracture features (through dimple number density) with strain rate dependent tensile properties.

It is known that the dislocation density (ρ) of a material varies during deformation and this is the controlling parameter of the mechanical behaviour of a metal. Dislocation density can be calculated by various methods like Transmission Electron Microscopy (TEM) and other methods like X-ray (XRD) or neutron diffraction [5-6]. It is known that TEM reveals material's features from very small area of specimen. Neutron diffraction on the other hand, is relatively newer technique but not always easy to access. X-ray diffraction method, however, is easy to adopt as well as this reveals the average data over a comparatively large area of a specimen which is exposed to irradiation. Further, the specimen preparation for TEM studies is difficult. In addition, the thinness of TEM specimen sometimes results in low dislocation density [7] with erroneous estimations. On the contrary, the preparation of specimen for studying X-ray diffraction (XRD) is easy and less time consuming. XRD is suitable for estimating dislocation density (ρ) of a material more exactly. Accordingly, X-ray diffraction (XRD) profile investigation is used for a variety of specimens such as polycrystalline materials and bulk single; single phase materials and polycrystalline powders to reveal various result such as dislocation density; crystal size and dislocation character[8-9].

## 1.2 Objectives

With the background available, the objectives of the present work are

(1) To characterise the investigated steel in respect to its chemical composition, microstructure and hardness.

(2) To determine the tensile properties of C-Mn440 steel at varying strain rates; from $10^{-4}$to1 strain rate using special universal hydraulic testing machine and for 10 to $10^{2}$using high speed servo-hydraulic testing machine.

(3) To analyze the fracture surfaces of the investigated C-Mn440 steels examined under different strain rate.

(4) To examine the mechanism of deformation in investigated steel by examining damage accumulation

(5) To examine the sub structure formation in deformed steel.

## 1.3 Lay out of the work

This thesis contains five chapters. The requirement of related experiments along with significance of the problem is described in **Chapter-1**. Literature background related strain rate variation and subsequently deformation behaviour of investigated steel in **Chapter-2**.The information which is available in the literature generates many queries and provides the directions for further research. The present study has been inspired by the achievements of the previous investigations. Details of test procedures material characterization, chemical composition analysis, microstructure analysis, hardness, test conditions and factors affecting tests have been discussed in **Chapter 3**. Obtained results on microstructures, hardness, and tensile test at varying strain rate and damage accumulation in **Chapter 4**. Conclusions derived from this work are summarized briefly in **Chapter-5** together with some proposed future work related to this area.

# CHAPTER .2

# Literature review

## 2.1 Introduction:

The present chapter contains to the present investigation material chosen for this investigation is carbon manganese steel .its properly microstructure discusses in the initial part of the chapter after this a compilation of the literature pertaining to the deformation behaviour of metals subjected to varying strain rates. High strain rate regime, its significance, standard testing techniques and various deformation mechanisms during high strain rate tests have been discussed in the following sections.

### 2.2 Carbon-manganese steel:

For the idea of increase the hardness toughness and strength manganese content in carbon steel is increased. Carbon manganese steel containing the manganese over 1.2% up to approximately 1.7%.The different grade of steel like grade300, AS3679,AS1442/1320and CMn440 steel are example of carbon manganese steel.

These are extensively used in engineering and manufacture industries and are highly durable with a long service life. Carbon-manganese steel is a high-strength low-alloy formable steel with enhanced fatigue performance. For the full fill meant the need of automotive industry for stronger, lighter components. The use of carbon-manganese steel means an increase the strength of the finished component or a reduction in the thickness of the steel or both .Down-gauging provides the added benefit of increased output per tonne of steel.

## 2.3 Microstructure of carbon manganese steel:

The basic material properties largely extent depend on the combination of the morphology of microstructure and grain size, after each plastic deformation step, it depends on the how much amount of the deformation temperature, plastic deformation of the material, and varying strain rate. In the carbon manganese steel, polygonal ferritic structure was obtained by quenching or

coiling, and also a narrow allocation of grain sizes with (Fig.2.1a and b). If the temperature is decreasing the at the final temperature to immediately above Ar3 this resultsis found in a finer grain size , but the polygonal grain size are looking properly. The finishing temperature of the coiled sample is 800℃, it is revels the bimodal grain size distribution (Fig. 2.1a). larger grains are situated after to Small grains. In the quench sample (Fig.2.1a) The bimodal grain size allocation can be investigated. The deformation temperature of the material 800℃ followed by quenching, it revels in microstructure like recrystallised ferrite grains, some hardening this micrograph show the deformed ferrite grains [10].

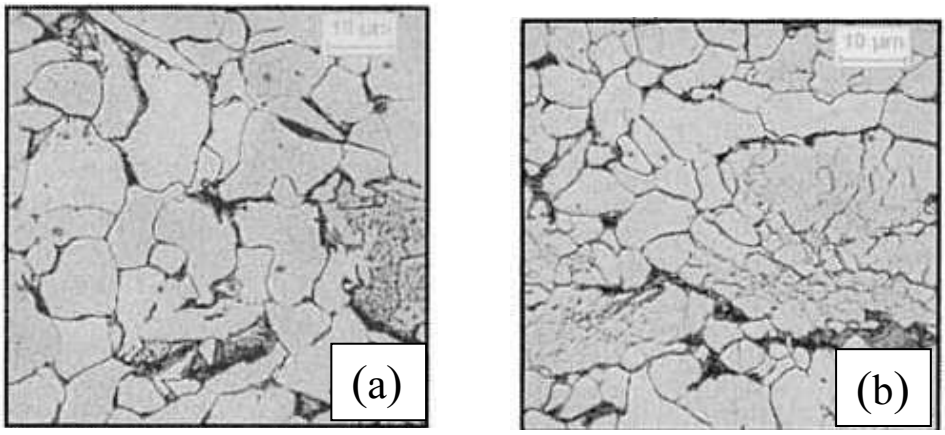


Fig.2.1.Optical micrograph of C-Mn (a) coiled rolled and (b) quenched sampled at (900℃)

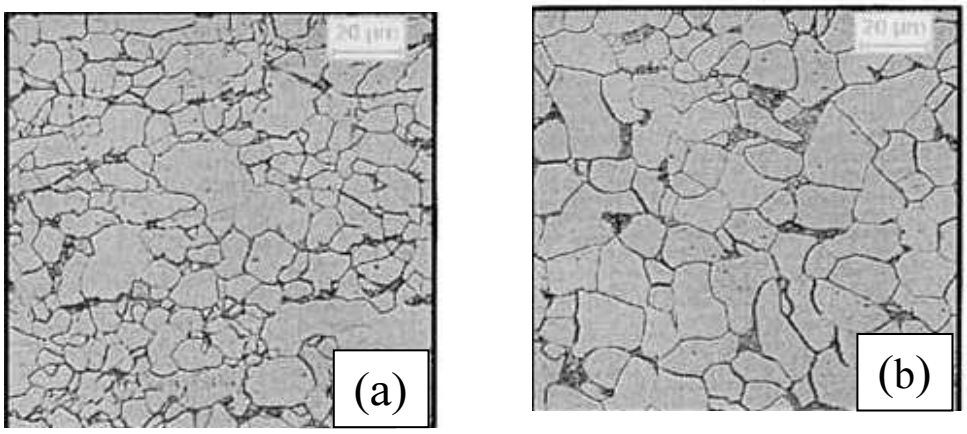


Fig.2.2. Optical micrograph of C-Mn (a) quenched sampled and (b) coiled rolled sample(800℃)

In carbon manganese steel normally ferrite and perlite phases are present.

## 2.4 Strain rate:

Strain rate is defined as $\dot{\varepsilon} = d\varepsilon/dt$. The conventionally units of strain rate expressed as $s^{-1}$, i.e. per second. During the extension of any cylindrical or flat body but here discusses only for cylindrical specimen with one end fixed and the other end attached to a movable crosshead of fixed velocity or constant velocity , the crosshead velocity, $v$ is expressed as $v = dL/dt$. The conventional linear strain rate expressed in terms of is $\dot{e}$ [1].

$$\dot{e} = \frac{de}{dt} = \frac{d(L - L_0)/L_0}{dt} = \frac{1}{L_0}\frac{dL}{dt} = \frac{v}{L_0} \tag{2.1}$$

The $\dot{\varepsilon}$ true strain rate is expressed as,

$$\dot{\varepsilon} = \frac{d\varepsilon}{dt} = \frac{d[\ln(L/L_0)]}{dt} = \frac{1}{L}\frac{dL}{dt} = \frac{v}{L} \tag{2.2}$$

Where, and L is the instantaneous length, $L_0$ is the gauge length. Equation (2.2) indicates that for constant crosshead velocity the true strain rate decreases as the specimen elongates. The strain rate is defined as at rate which strain is applied to specimen. Strain rate have an important influence on the flow stress.

Table.2.1.Range of strain rates

| **Range of strain rate** | **Condition or type of test** |
|---|---|
| $10^{-8}$ to $10^{-5}$ $s^{-1}$ | For the Constant load test like Creep test or stress. |
| $10^{-5}$ to $10^{-1}$ $s^{-1}$ | For the Hydrostatic tension test or screw driven machines |
| $10^{-1}$ to$10^{2}$ $s^{-1}$ | For the Dynamic tension or compression |
| $10^{2}$ to $10^{4}$ $s^{-1}$ | For the High speed testing using impact bar |
| $10^{4}$ to $10^{8}$ $s^{-1}$ | For the Explosively driven projectiles (shock-wave propagation) or hypervelocity impact using gas guns |

Conventional strain rate is proportional to the cross head velocity. In modern testing machine the cross head velocity can be set accurately and controlled easily. It is a simple matter to perform tension at fixed conventional strain rate.

## 2.5 Effect of strain rate on flow stress:

It is also known that with increase the strain rate increases flow stress. Moreover the strain rate mostly dependence of mechanical strength increases with increase in temperature of the material. The flow stress and yield strength at lower plastic region strains (Plastic strain) are more dependent on strain rates. [1]

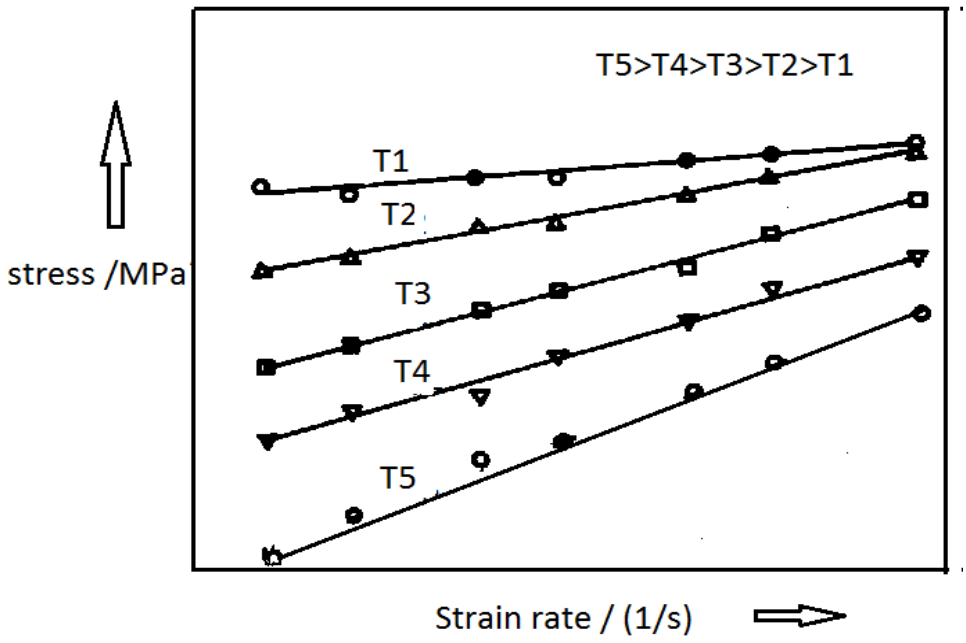


Fig.2.3.Flow stress versus strain rate for aluminium alloy

It is clearly seen that from above figure strain rates dependent on strength and temperature. From the closer view of figure.2.3 clearly shows that slope is increasing with temperate. High rate of strain causes the yield point to appear in tests for the low carbon steel material does not show a yield point under normal rate of loading [1]. From table.2.1 are clearly shows that different testing ranges like low medium and high strain rates. It is important to understand about high strain rate because the deformation of automotive body is at very high speed impact it mines at high strain rate.

## 2.6 High strain rate:

### 2.6.1 Significance of high strain rate testing

In structural applications, various components have been designed to function over a large range of strain rates. Moreover, in metal working operations materials are subjected to a large amount of strains at different strain rates and temperatures. Mechanical behaviour at high strain rates differ significantly from that investigation at quasi-static or intermediate strain rates, and many engineering applications require characterization of mechanical behaviour under dynamic load conditions. For example, strain rates ranging from100 $s^{-1}$ to more than $10^4$ $s^{-1}$ occur in many processes or events of practical importance, such as automobile crash, foreign object damage, earthquakes, blast loading, explosive forming, , terminal ballistics, metal working and structural impacts. High strain rate testing is performed to determine mechanical properties of materials which are subjected to deform at large range of strain levels and strain rates throughout various structural and forming operations.

### 2.6.2 High strain rate testing technique

Generally, determination of tensile properties (Yield Strength(YS), Ultimate Tensile Strength(UTS), total elongation and uniform elongation) using quasi-static loading of any material is performed at strain rates of $10^{-3}$ to $10^2$ $s^{-1}$ (nominal to intermediate strain rate) using servo hydraulic testing machines. But dynamic tensile properties of these materials are determined at strain rates above$10^3$ $s^{-1}$ (high strain rate). These high strain rate testing cannot be performed using the conventional testing machines used for quasi-static loading, due to their limitations to cross head velocity. A modified Split Hopkinsons Pressure Bar apparatus is currently used for tensile and compression testing of materials at high strain rates. Fig2.4 shows the various strain rate regimes and their associated instruments. Apart from split Hopkinson tensile bar set up, other specialized technique for high strain rate

tensile testing has been also used, which are, expanding ring test, flyer plate and short duration pulse loading and rotating wheel.

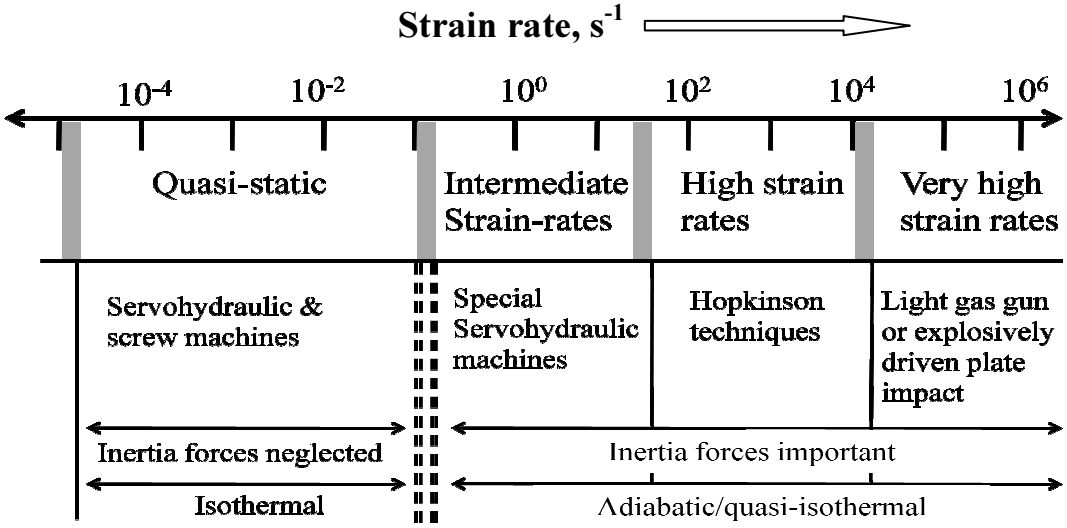


Fig. 2.4: Strain rate regimes and associated instruments (ASM, 2000[11])

### 2.6.3 Dynamic factors at high strain rates

A primary difference between a quasi-static test ($10^{-5}$ to $10^{-1}$) and a high strain rate test ($10^{2}$ to $10^{4}$) is that first is inertia and second is wave propagation effects become more definite at higher strain rates. These dynamic effects on test results become highly definite at higher strain rates for low, medium, high, and very high strain rate regimes. When the strain rate is varying through the medium strain rate regime, the observation of load is the first to be influence by stress wave propagation. Uniform plastic deformation within the specimen becomes more crucial if the strain rate is increased. At very high strain rates beginning at in range about $10^{4}$ or $10^{5}$ $s^{-1}$, critical shock wave propagation [11].

### 2.6.4 Effect of high strain rate on microstructural properties of metals

In any deformation process, some part of work done during deformation transforms into heat which gets released from the sample during testing under quasi-static condition, but it cannot leave the sample in case of high strain rate deformation processes since the time to deformation is very less (generally some micro second) and thus it leads to 'adiabatic heating'. During deformation of metals at quasi-static condition, plastic deformation at low strain (0-0.5) is described by simple dislocation theory, [12] and complex dislocation interactions along with sub-grain formations explain the deformation behaviour at large plastic strains (strains > 1) [12].But, in high strain rate, plastic deformation is accompanied by adiabatic heating which leads to thermal softening along with strain hardening at large plastic strains.

Apart from thermal softening, microstructural changes occur within the material due to adiabatic heating during high strain rate deformation processes if the alloy is heat treatable, whereas for non heat treatable alloys, thermal softening is the only dominant characteristic (Marchand, 1988). From the successive investigations of Odeshi et. al. (2005), Marchand et. al. (1988), Rogers and Shastry, Meyers and Wittman etc., [12,13,14,15]. it has been found that adiabatic heating during high strain rate deformation of pearlitic and martensitic steels, in various quenched and tempered conditions lead to the formation of adiabatic shear bands. These narrow shear bands causes extreme strain localization during complex deformation process at very high strain rates[12]. Shear bands are also found in low strain rate deformation process but the term adiabatic is used when the strain rate is greater than $10^2$ $s^{-1}$. The concept of adiabatic shear bands was first proposed by Zenner and Hollomon [16].

Adiabatic shear bands can be broadly classified as 'transformed' or 'deformed' shear bands, as proposed by Timothys, 1987 [17] on the basis of their metallographical appearance. Transformed shear bands form due to permanent change in the microstructure during the

local straining process where the intense heat produced in the local region is quenched rapidly by the surrounding material. The distinct microstructure of transformed shear bands in steels has been shown to be mainly martensitic in nature. Thus the term 'transformed' is primarily associated with the permanent phase transformation which occurs within the material. The deformed shear bands are basically zones of intense shear deformation of the original microstructure where no phase transformation of the original microstructure takes place, as shown in Fig 2.5.

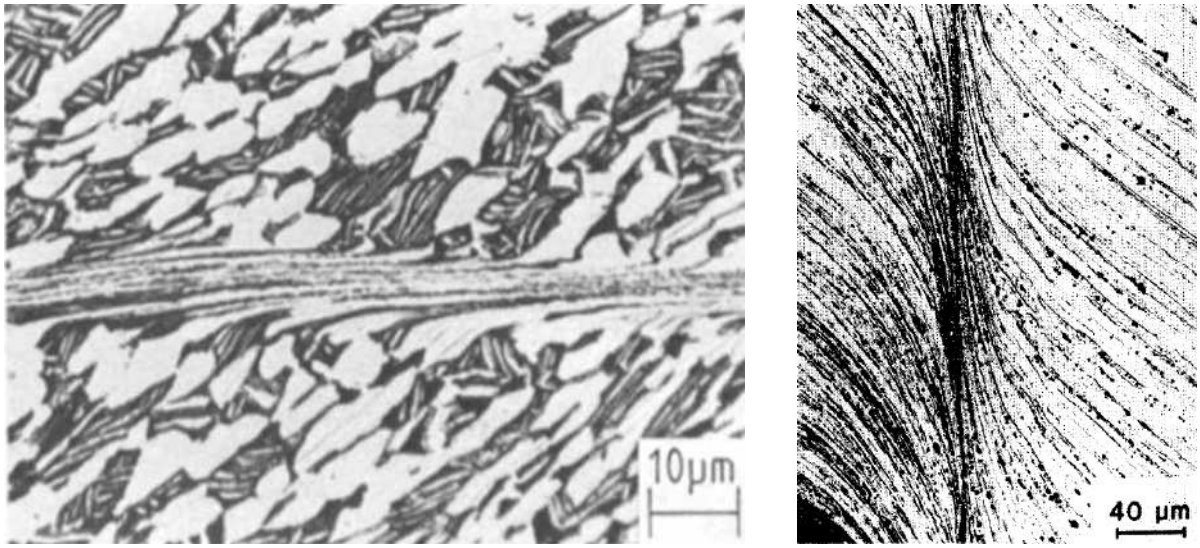


Fig. 2.5 (a) Transformed shear band in hot rolled Ti-Al alloy, (b) Deformed shear band in 7039 Aluminium alloy[17].

### 2.6.5 High strain rate behaviour of high strength steels

Due to wide use of high strength steels like TRIP, TWIP ,ultra high strength, steels, DP steel C-Mn steel etc. in automobile car bodies, various investigators have successfully analyzed the dynamic tensile stress strain behaviour of these steels. Among these steels the effect of strain rate has been extensively studied on TRIP, TWIP, DP steels etc. [18-19] due to their high toughness. In a study by Wei et. al.(2007) [18]. It was found that strength of TRIP aided DP steels increases remarkably with increasing strain rates. In an another study with 304 LN stainless steel, it was found that 304 LN stainless steel exhibit

Table.2.2.Critical review of published literatures correlating mechanical properties with varying strain

| Researchers | System | Year/journal | Remarks |
|---|---|---|---|
| Song Ren bo and Dai qi fong . | DP steel | 2013/ J. Iron. Steel Res. Int. | DP –steel is strain rate sensitive and ultimate tensile (UTS) strength and yield strength (YS) increase with strain rate. |
| Luo Yung-Rong et al | High strength structural steel | 2013/ J. Iron. Steel Res. Int. | Fatigue life of steel manly depends on strain rate. |
| Jingui quin et al | DP700&DP500 steel | 2013/ J. Mater. Sci.A | DP700 steel shows higher value of strength and lower value of ductility compare to DP500 steel under quasi static and high strain rate loading. |
| Zong Ping He et al | TRIP steel | 2012/ J. Mater. Sci. Technol. | For TRIP steel, with increasing strain rate, first tensile elongation decreases of TRIP steel and then increases. |
| Ji–hoon kim et al. | DP780,DP980 TRIP 780 | 2012/J.Mater. Sci. &Eng | Strain rate dependent plastic flow stress behaviour in YS,UTS,and total elongation. |
| George T gray 3 | Alloy and metal | 2012/J.Mater.Sci and Techno.Divi . | Deformation at higher strain rate where the higher strain rate sensitivity can lead to high stress and point defect increase. |
| Si woo Hwang et al | Fe-22Mn-xAl-0.6C steel(austenitic high Mn steel) | 2011/J.Mater. Sci& Eng | At high strain rate UTS decrease with increase with aluminium percentage .0%Al has more strength compare to 6% Al content in austenitic high Mn steel. |
| Akihiro Uenishi | Multi phase steel (DP,TRIP) | 2011/J.Automotive Engineering | The multi phase steel like DP and TRIP steel have superior strain rate sensitivity of flow stress as compared to the single phase steel. |
| Xiong rong gang et al. | TWIP steel at high strain rate. | 2009/ J. Iron. Steel Res. Int. | TWIP steel is strain rate sensitive. With increase of strain rate increases the yield strength(Y.S) and ultimate tensile strength (U.T.S) and uniform elongation decrease. |
| Y.s kim et al. | High nitrogen austenitic steels. | 2007/J. Mater. Proc.technol. | The high nitrogen steel strength increases with increase the nitrogen content and increase UTS , YS. |
| C. girish shastry et al | 2.25Cr-1Mo steel | 2007/ J.Mater. Sci& Eng | The strain rate sensitivity increases with increasing temperature and strain. |
| | | | |

| | | | |
|---|---|---|---|
| Hoon hul et al. | TRIP and DP steel | 2007/J. Mech. Sci. | Flow stress increases with varying strain rate strain rate for both DP and TRIP .DP steel are more strain sensitive then TRIP. |
| Ding Hua et al. | Fe-mn-al,low carbon high manganese steel(TRIP,TWIP) | 2006/ J. Iron. Steel Res. Int. | With increase of Mn%(33%) elongation is increase but UTS is decrease and at low manganese (23%)higher strength increases the UTS,YS. |
| M A Saaki itabasi and Kozo kawata | Carbon steel | 1999/J.Impact Engineering | As carbon percent increase from (0.14to0.54) the UTS increases and Y.S at high strain rates . |
| Woei-shyan lee et al | AISI 4340 alloy steel | 1995/J.Mater Proce.Technol. | Flow stress (MPa) increase with as well as increase in strain rate(1/S) or decrease with temperature. |

high strain rate sensitivity and its flow stress increases with strain rate (Lee and Lin, (2001)). The increase in flow stress with increase in strain rate is governed by the equation: q = bqv, where, b is the Burger's vector, q is the mobile dislocation density and v is the average dislocation velocity [1]. To maintain the higher imposed strain rate, v needs to be increased with instantaneous increase in flow stress [1].

## 2.7 Strain rate sensitivity:

The strain rate sensitivity describes the dynamic material behaviour, and is therefore an important mechanical property to be determined ([20], [21]). The strain rate sensitivity is defined by its relation to the plastic flow curve, and not to the engineering stress-strain curve. The definition of the strain rate sensitivity is indeed based on true stress values, not on engineering stress values. For this reason, the tensile strength cannot be used as such, since this is an engineering stress value. Only the yield strength (0.2% plastic strain)can be used directly, since it corresponds approximately to the flow stress value $\sigma_{true}$,0.2%.

There are many definitions available for the strain rate sensitivity in the literature. Jump tests are used to deliver the instantaneous value of strain rate sensitivity, without taking into account the strain path history [22]. The concept of dynamic factors has been used in [23] for example, as the ratio of dynamic to quasi-static values, for the yield and tensile strength. The difference between dynamic and quasi-static tensile strength has been determined as an alternative in [24] in order to compare the strain rate sensitivity of the tensile strength for a wide range of materials .The strain rate sensitivity is however calculated in most publications based on the strain rate dependency of flow curves. The logarithmic strain rate sensitivity m is originally defined from the extended Hollomon equation (2.3) as follows [25].

$$\sigma = K \varepsilon^{\nu} \dot{\varepsilon}^{\mu} \qquad (2.3)$$

When defining the strain rate sensitivity, the difference between natural (basis e) and decimal logarithm (base 10) has to be done. Furthermore, the strain rate sensitivity can be defined, based on the logarithmic strain rate, in a semi-logarithmic or logarithmic way, Table2.3.The semi-logarithmic strain rate sensitivity corresponds to the dynamic flow stress increase, when the strain rate is multiplied by 10 with one order of magnitude increase. This is experimentally meaningful, since significant effects on the flow stress, beyond usual results scattering, can only be seen when the strain rate is multiplied by 10. For this reason, the strain rate has to be represented in a logarithmic scale. The strain rate sensitivity is related to both true plastic strain and strain rate considered. The natural logarithmic strain rate sensitivity me is also very often used, mostly for modelling purposes. Both10 and m are considered later on in this investigation [40].

Table.2.3. Strain rate sensitivity definitions.

| | | |
|---|---|---|
| Natural semi-logarithmic strain rate sensitivity βe | $\beta e=\delta\sigma/\delta(\ln(\dot{\varepsilon}))$ | (2) |
| Semi-logarithmic strain rate sensitivity $\beta_{10}$ | $\beta_{10}=\delta\sigma/\delta(\log_{10}(\dot{\varepsilon}))$ | (3) |
| Natural logarithmic strain rate sensitivity $m_e$ | $m_e=\delta(\ln(\sigma))/\delta(\ln(\dot{\varepsilon}))$ | (4) |
| Logarithmic strain rate sensitivity $m_{10}$ | $m_{10}=\delta(\log_{10}(\sigma))/\delta(\log_{10}(\dot{\varepsilon}))$ | (5) |

## 2.8 Ductile fracture behaviour:

### 2.8.1. Mechanism of ductile fracture:

Detail study of the ductile fracture process shows that a central crack which forms easily tends to concentrate the deformation at the tip in narrow bands of high shear strain.These shear band at angles of 50to60° to the transverse direction. Sheets are void are nucleated in these band, and the void grow and coalesce in to local fracture of void sheet .while the average direction of crack growth is radially out ward in direction transverse to the tensile axis, on finer scale the crack zig-zags back and forth across the transverse plane by void-sheet formation. Thus crack growth in ductile fracture is essentially by a process of void coalescence. Coalescence occurs by elongation of void and elongation of fracture surface consisting of elongated “dimples”, as if it had formed from numerous holes which was separated by thin walls until it fracture.

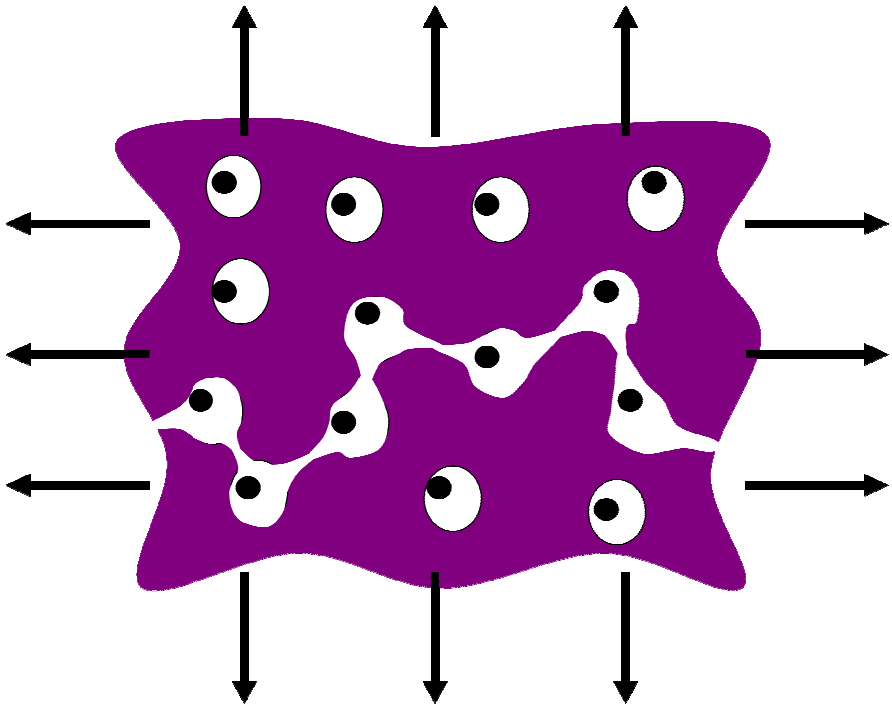

Fig.2.7.Mechanism of ductile fracture

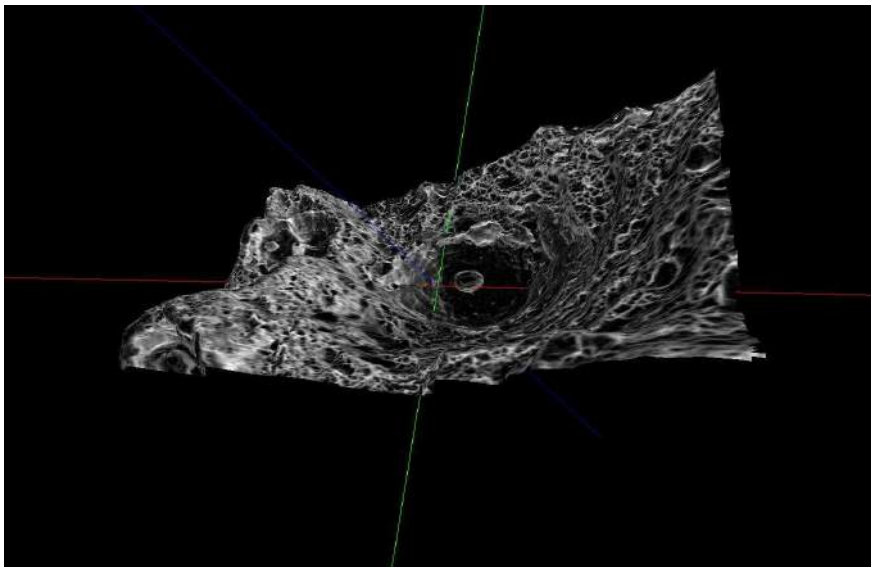

Fig.2.8Ductile fracture

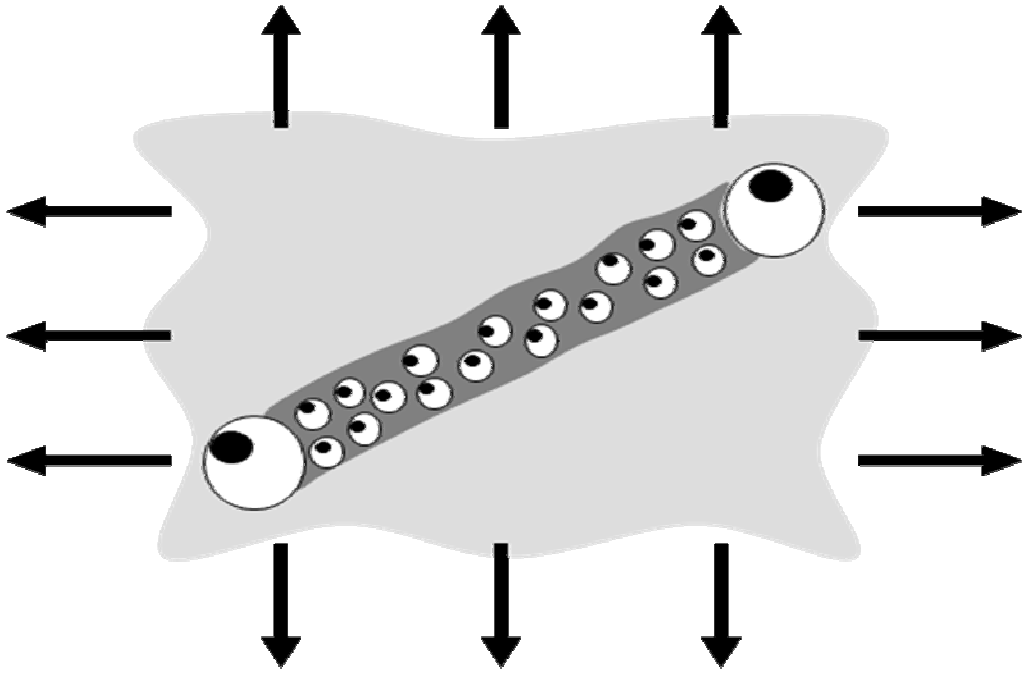

Fig.2.9. Void sheet Formation

Particles and inclusions are not all of same size.Different type of particles provide differing resistance to void nucleation.It is particularly difficult to nucleate voids at fine particles.Strain localisation between growing bigger voids trigger the nucleation of voids at smaller particles.Since the smaller particles are numerous, they coalesce without requiring to grow much.

## 2.9 Dimple geometry:

Figure.2.10 represent that the mean size of the dimples constituting the keep going fracture movements depending on the strain rate. It is clear from the Figure 2.10 the dimple size is small at the low strain rate but at a high strain rate the dimple size increases.[26-27-28] From Figure 2.11 it is obtained that distribution of dimple size studied for all the strain rates, revealing that, for strain rates of $10^{-4}$, $10^{-3}$ and $10^{-2}$ $s^{-1}$,for the largest production of approximately 0.50 µm diameter of dimples was found. After this the dimple distribution is almost not varying. Common range of dimple size was found in between around 0.35µm and

0.65 µm. At increasing strain rate dimple size increases. as discusse din d.etail elsewhere [27-28].

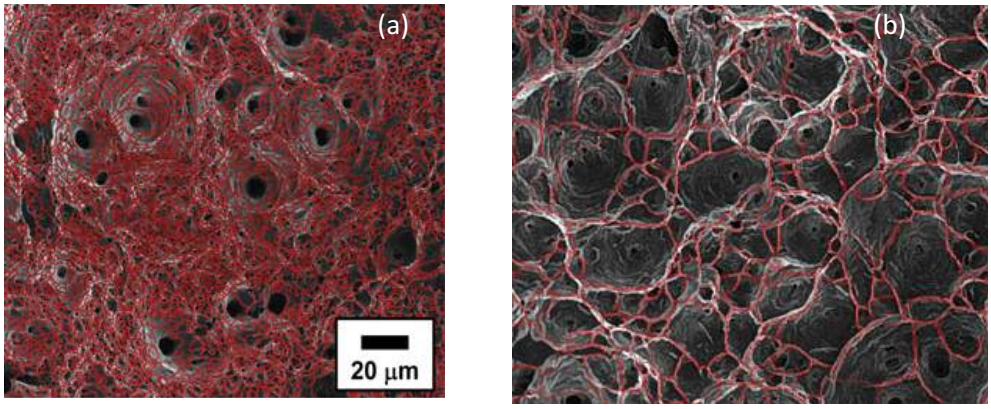


Figure.2.10.Dimple network by SEM image at strain rates of (a) $10^{-4}s^{-1}$and (b) $1s^{-1}$.[28]
.

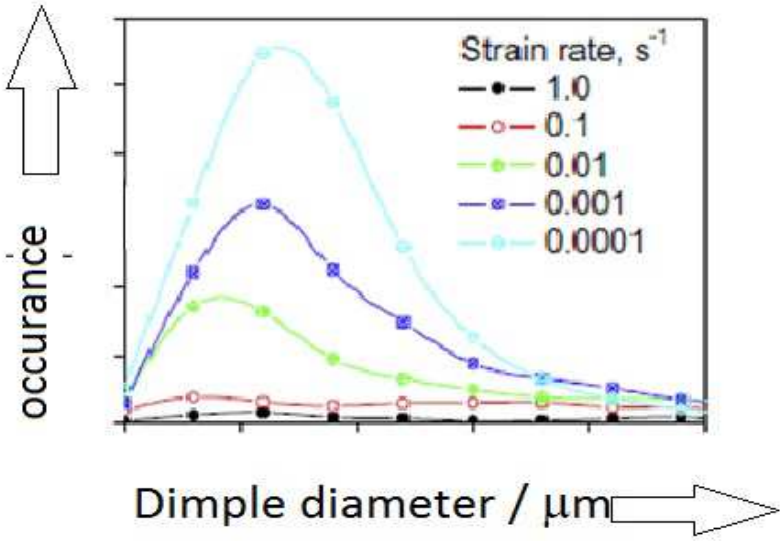


Figure2.11. Size distribution of Dimple on fracture surface at varying strain rates

## 2.10. Effect of strain rate on void nucleation:

Continued fracture a surface is formed by voids grow, Stress state, coalesce. By this way finally form the dimples. The dimples easily generates where the secondary phase particles or inclusion presents. However Inclusions was play Important role in this failure process, still though they are present in a comparatively small quantity [29]

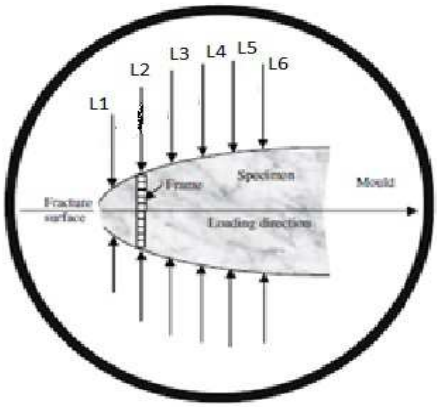


Fig.2.12. Line diagram of mould metallography sample

How the dimple diameter for the cylindrical sample present for investigation at the range of strain rates are shown in Figure 2.12. It is investigated by the Arpan etal. that the with increasing the strain rate the mean dimple diameter increases. if strain rate ($0.0001s^{-1}$) for minimum strain rate the dimple diameter is minimum.it is investigated by Arpan et al. an correct fractographic study can be used to make a good estimation of the deformation behaviour of the material and variation in the mechanical properties [27].

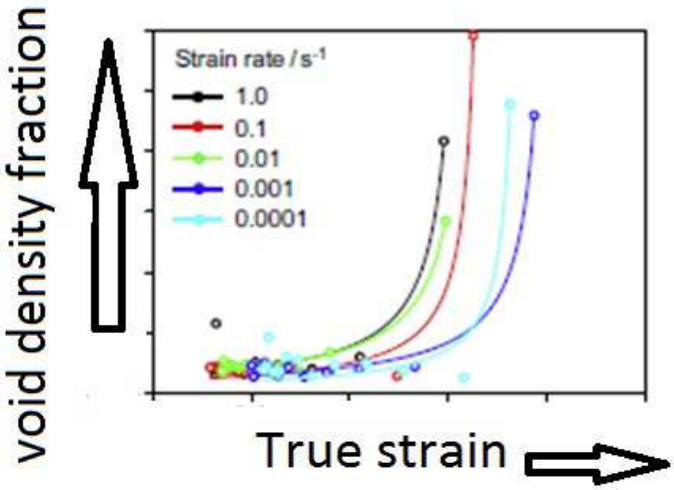


Figure.2.13 Void density fraction verses true strain diagram at varying strain rate. [26]

From Figure 2.13, it is clear that voids initiate much faster in the higher strain rate specimen than in the lower strain rate.

## 2.11 Dislocation density by x-ray diffraction

Dislocation density is defined as the number of dislocations in a unit volume of crystalline material. It can be calculated by direct or indirect methods like Transmission Electron Micro- scopy (TEM) and indirect methods like X-ray (XRD) [30].

### 2.11.1 Process of dislocation density calculation

For the calculation the dislocation density the modified Williamson–Hall equation [30] is use in order to calculate the dislocation density in the ferrite and martensite phases in the steel under examination at normal room temperature. Now the strain broadening is caused due to the presence of the dislocations which is generated during deformation of material. For the calculation of full width at half maximum (FWHM) of diffraction profiles can be expressed by the modified William- son–Hall plots [31].

$$\Delta K \cong 1/d + \left(\frac{\pi M^2 b^2}{2}\right) \rho^{\frac{1}{2}} (K^2 \overline{C}) + O(K^4 \overline{C^2}) \qquad (2.4)$$

where,

$\Delta K = \cos\theta(\Delta 2\theta)/\lambda$ $K = 2\sin\theta/\lambda$

$\theta$ = diffraction angle and $\Delta(2\theta)$ =integral breadth (Full Width Half Maxima ) of the diffraction peak

$\lambda$ = wavelength of the X-rays d = average grain size

b = magnitude of the Burgers vector of the dislocations and $\rho$ = average dislocation density

M is a constant which depending on both the effective outer cut-off radius dislocation density and the dislocations .For the deformed material the value of M in between 1 and 2 [32, 33]. Normally the value of M=2 is used for all the steel material subjected

deformation in the present study. C is the average contrast factor of the dislocations for a particular reflection.

$$C = C_{h00}\left[1 - q\left(\frac{(h^2k^2+k^2l^2+l^2h^2)}{h^2+k^2+l^2}\right)\right] \qquad (2.2)$$

Where $C_{h00}$ = average contrast factor consequent to h00 reflection. Ch00=0.266 is obtained from the published paper by Ungáretal et al. The value of q=2.203 is calculated based on the

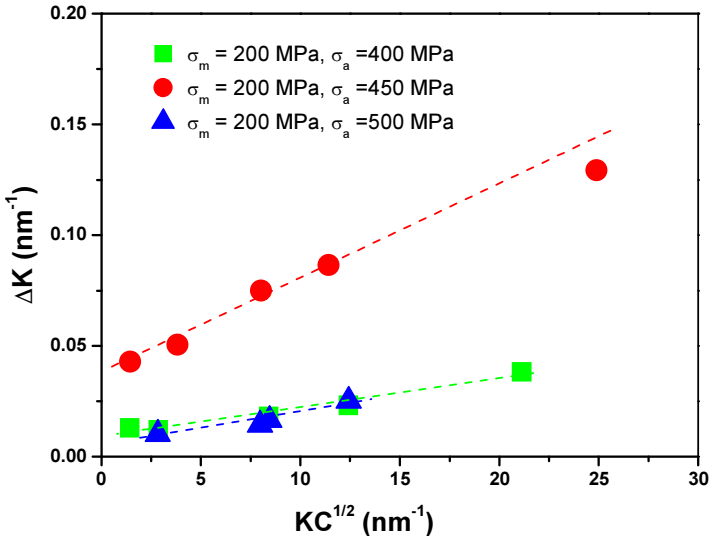


Fig 2.14.Modified Williamson–Hall plot for Peak broadening analysis.

expression [30]. Now two important microstructural features provided by modified Williamson–Hall plot. The intersection at K=0 of the linear fit of the curves provide the average grain size (1/d) or the diffraction domain size. The m =slope of the fitted curve .it is used for the calculation of dislocation density from the given below equation [30].

$$\rho = \frac{2m^2}{\pi M^2 b^2} \qquad (2.3)$$

The ΔK vs. $K^2C$ plot give the slope (m) value from the linear fit of the data points.

# CHAPTER .3

# MATERIAL, EXPERIMENTAL DETAILS AND TESTING PROCEDURES

## 3.1 Introduction

The aim of this investigation is to study the different strain rate deformation behavior of Carbon manganese 440 steel, in conjugation with the investigations related to deformation at different strain rate. In this chapter are described to fulfil these aims, different kinds of experiments. An outline of all the experiments includes determination of chemical composition of the investigated steel, microstructural characterization, determination of tensile behavior of the steel at high strain rate, study of facture surfaces, damage accumulation, effect of strain rate on grain size, x-ray analysis at different strain rate.

## 3.2 Material Selection

The selected material for standardizing the high strain rate test technique was C-Mn440 steel. Desired sheet samples for conducting the different strain rate tensile tests were obtained from TATA steel which is provided by NML. The dimension of the sample used in quasi-static strain rate testing is given in Fig 2. As received sheet material is known to be cold rolled. The chemical composition of the material has been given by optical emission spectroscopy and is listed in Table 1.

## 3.3 Chemical composition:

The chemical composition of the investigated steel was determined by using optical emission spectrometer (model: ARL 3460 Metals Analyzer, Thermo Electron Corporation Limited, Switzerland).

## 3.4 Metallography

These were first polishing by silicon carbide paper at different grades (230-400-600-800-1200-1500-2000), followed cloth polishing by using of alumina and silicon colloidal solution.

The polished specimens were etched with 2% Nital for 10 s .The microstructural examinations were carried out with the help of optical microscope (Model: Olympus BX61, Tokyo, Japan), which is connected to an image analyzer.

### 3.4.1 Optical Microscopy

Samples of approximately 10mm x 6.5mm x 1.5mm size were cut from the as received material for metallographic inspections. These samples were first roughly ground on belt grinder. The specimen was made to move perpendicular to the existing scratches on the belt grinder it was continued until the surface is flat and free of nicks, burr etc. after this all corner are chamfer. After rough grinding, the samples were ground with rotating discs of abrasive paper, i.e., wet silicon carbide paper. The coarseness of the paper is indicated by a number .The grinding procedure involves several stages, using a finer paper (higher number) for each successive stage i.e. from 80, 120, 180, 220, 320, 400, 600, 800, 1000, 1200and 2000. Each grinding stage removes the scratches from the previous coarser paper. This was more easily obtained by orienting the specimen perpendicular to the previous scratches, and watching for these previously oriented scratches to get obliterate. Samples were thoroughly washed with soapy water and then allowed to dry. The final scratch-free surface was obtained by using a rotating wheel (Fig 3.1) covered with a special cloth that was charged with abrasive particles. The abrasive either using diamond paste of particle size of 1µm and 0.25µm or using colloidal suspension of beta alumina having particle size of 0.25µm and 0.1µm. The cloth used in our case was velvet cloth. After fine polishing samples were thoroughly cleaned with soap solution, and subsequently dried using drier. Samples were etched with 2% Nital (98%$C_2H_5OH$+2%$HNO_3$) solution.


Figure3.1 Rotating disc for paper polishing

### 3.4.2 Optical Microscopy

The polished and etched metallographic specimens were studied using an optical microscope (LEICA DM 2500M (Fig. 3.2)). The software used is LAS V3.6 .These examinations were carried out in three directions (R-D,T-D) at different magnifications and several representative microstructures of the specimens were recorded

Figure 3.2Optical Microscope

### 3.4.3 Grain size measurements

According to ASTM standard E-112 [35] the average grain size of the CMn440 steel was determined by use of the linear intercept method. In the linear intercept method, a linear test grid was drowning on the microstructure and the number of grains boundary intercepted by the test line was counted. Such measurements don at a magnification of 500X. The average grain size was then calculated using the relation:

Grain size (d) $=L_T/N_L$.....(3.1)

Where,

$N_L$ is the number of grains intercepted by a unit true test line length.

$L_T$ is the true length of a test line is defined as the length of the test line at unit magnification.

## 3.5 Hardness Determination

The samples prepared for hardness measurements were first made flat and parallel to opposite faces using a belt grinder to ensure precision of measurements. The samples were then mechanically polished using the procedure mentioned in section 3.2. Hardness was evaluated in three directions, with the help of a Vickers Hardness Tester (Model: Leco LV 700, (Fig. 3.3).

Figure 3.3Leco LV 700 Vickers hardness testers.

The hardness was measured at the load of 30kgf. Minimum 3 readings were measured for each particular sample to calculate the average micro hardness.

## 3.6. Tensile Test:

### 3.6.1 Low strain rate sample (Quasi-static Tensile Testing)

Tensile tests of DP600 and DP800 steels have been performed in a servo-hydraulic UTM, at various strain rates ($0.001s^{-1}$, $0.01s^{-1}$, $0.1s^{-1}$ and $1\ s^{-1}$). The samples for these tensile tests were prepared following the ASTM standard E8M [36]. A 25 mm gauge length extensometer was used to measure the strain directly from the sample. The length of the specimens have been kept parallel to the loading direction of the sheets.

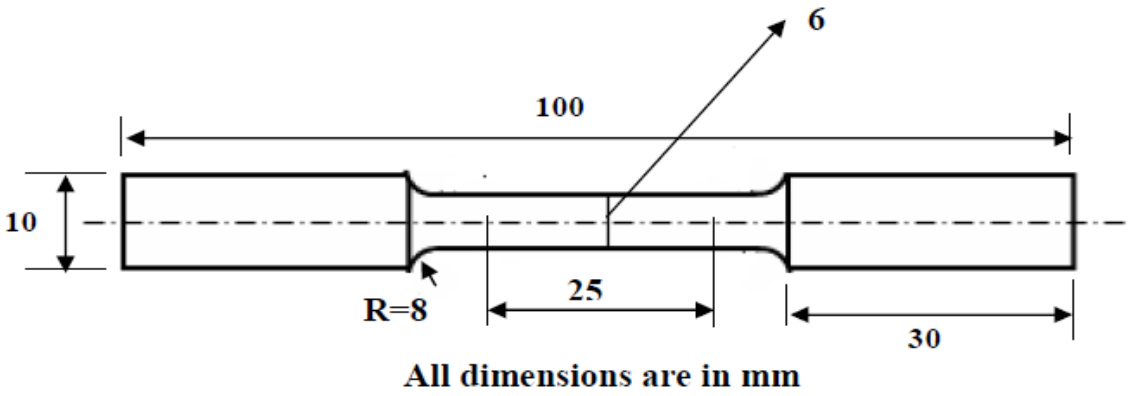


Fig. 3.4-Typical tensile test specimen for testing of quasi –static strain rate

.

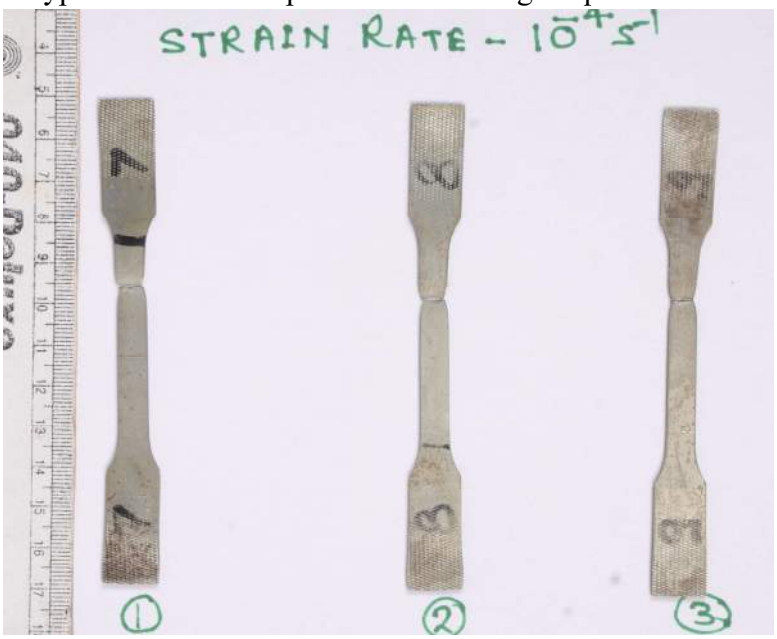


Fig 3.5 Quasi-static strain rate testing sample

## 3.6.2 High strain rate test:

High strain rate testing of the obtained samples are conducted in INSTRON VHS 8800 servo-hydraulic testing machine. The two samples were tested at crosshead velocities of 5,15, m/s. A typical test specimen for high strain rate tension test is shown in Fig 3.7.

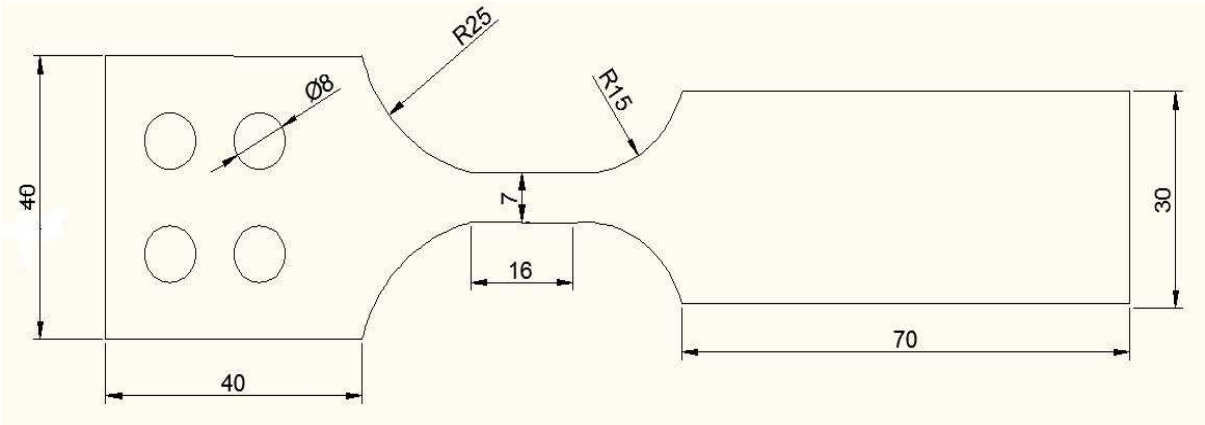


Fig. 3.7: Typical tensile test specimen for high strain rate testing

Where,
7mm is gage width of the sample, 16 is gage length of the sample,1.59is the thickness of the sample

For high strain rate test the above standard is fallow for the selected material. Now the gage length of the selected sample is 16mm and the width of the sample is 7mm and the thickness of the selected CMn 440 steel is 1.59mm.

*Piezoelectric load cell*

Fig .3.8 High strain rate testing machine

The uniform strain rates obtained were 100,400 for crosshead velocities of 5,15m/s respectively.

Table 3.1: Employed strain rates for high strain rate tests

| **Sl. No.** | **Velocity (m/s)** | **Strain Rate ($s^{-1}$)** |
|---|---|---|
| 1 | 5 | $1x10^2$ |
| 2 | 15 | $4x10^2$ |

## 3.7 Fractography with the SEM (Failure Analysis):

Fracture surfaces of materials study by the method of Fractography. This method is used to studying the characteristics of a fracture surface for find out cause of failure in engineering structures. In the ductile fracture the dimples are generated. And the size and density of dimple is affected by variation of strain rates. These dimple are examined by SEM. Fractography requires examination at a finer scale, which is usually carried out in a Scanning electron microscope or SEM shown in Fig. 3.7.

Figure 3.9 Scanning Electrons Microscope

The resolution of SEM is higher compare to the optical microscope, although samples are investigated in a partial vacuum at near atmospheric pressures. At very high load pulses as given for instance by a sequence of impacts, the striations can become visible to the naked eye and show a dimple structure in the SEM.

## 3.8 Voids measurement

. In this study, extensive investigation was carried out on the specimen sub-surfaces on planes along the specimen axis and parallel to the fracture surface using optical microscopy for building a relationship between strain rate and void formation at sub-surfaces. In view of this, specimens were cut after fracture using a slow speed cutter. Specimens were moulded for the ease of polishing as schematically illustrated in Fig.3 11. Starting from the fracture end of the specimens, a large number of fields (i.e. several optical images) were sequentially viewed under an optical light microscope along the lines $L_1$, $L_2$, $L_3$, $L_4$, $L_5$ and $L_6$ as shown in Fig. 3.10.

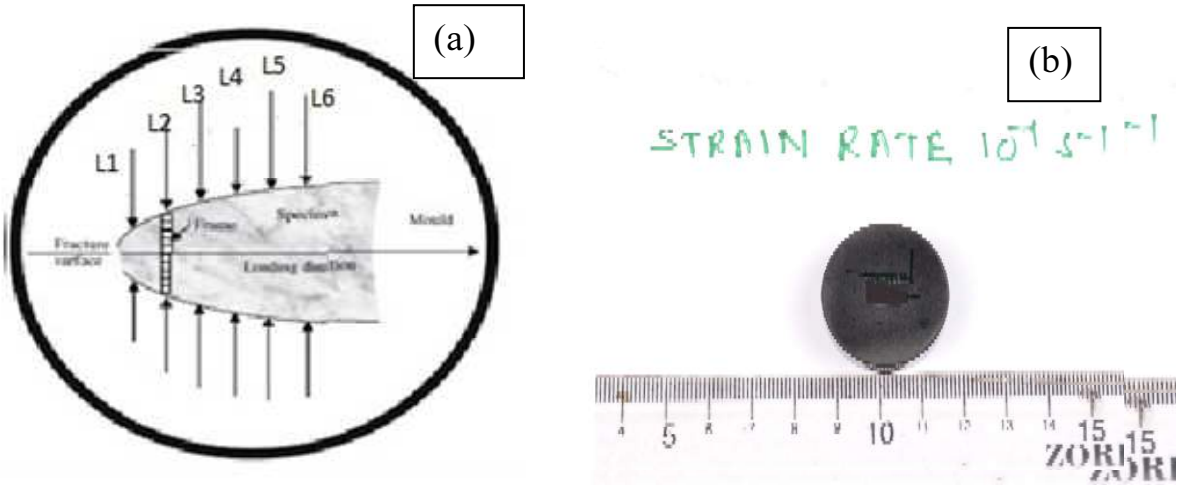


Fig.3.10 a) Schematic representation of metallography sample inside the mould calculating voids at different strain, (b) Actual material.

The microstructures along all these lines were digitally recorded with a magnification of 100×. It was found that the voids appear darker (i.e. black spot) in the bright background of ferrite matrix under the optical microscope. The true strain was estimated by measuring the width of the specimen at the specific transverse plane and making use of the relationship:

True strain $(\epsilon) = ln(w_o/w)$ [1], where $w_o$ and w are the original/initial width and the width at selected transverse plane respectively.

## 3.9 X-ray Diffraction

To investigate the possible structural alternations during tensile, tensile deformed specimens at varying strain rate like (0.0001,0.001.0.01,0.1,1$s^{-1}$ )were cut and these were subjected to X-ray diffraction (XRD) .The XRD analyses were carried out using high resolution Cu-Kα radiation(Model: XPert-3040Y00, Holland). For this investigation XRD in the scanning range of 20°-120° and scanning rate of 2°/min.


Fig 3.11 X-ray diffraction machine

# CHAPTER .4

# RESULTS & DISCUSSION

# 4.1 Material characterization

## 4.1.1 Material selection and Chemical composition

The material selected for this investigation is CMn440 steel. This is finds its application particularly in automobile sectors. Traditionally, steels used for automobiles are interstitial free (IF) steel and bake hardened (BH) steel, due to their high strength. However, the carbon manganese steel is also emerging into applications owing to its comparable high strength steel to IF, BH steel with relatively low cost. The name C-Mn-440 is given as the minimum ultimate strength is 440 MPa for this kind of steel.

**Table 4.1 Chemical composition of the CMn440 steel (all in wt%)**

| C | Mn | S | P | Si | Al | Cr | Ni | Nb | N (ppm) | Fe |
|---|---|---|---|---|---|---|---|---|---|---|
| 0.065 | 1.46 | 0.008 | 0.02 | 0.017 | 0.041 | 0.017 | 0.016 | 0.016 | 28 | Balance |

The chemical composition of the selected material is shown in Table 4.1. It contains 0.065% carbon with other major alloying elements of Mn, Ni, Cr and Nb as 1.46%, 0.016% 0.017% and 0.16% respectively. Usually the carbon manganese steel contains 1-1.5% Mn which is cold rolled during processing; on the other hand, hot rolled carbon manganese steel contains 0.4% carbon and 1 – 1.65% Mn, 0.15 – 0.40% Si [37]. In HSLA steels, 0.08% C, 1.3% Mn, 0.2% Nb and 0.05% V. The chemical composition of investigated steel is comparable with HSLA steel to a greater stent only difference in vanadium content. The estimated composition confirms the steel to be CMn440 grade steel as per specification given in ASM handbook volume1 properties and selection iron steel and high performance alloy1990 [37]. Manganese provides solid solution strengthening in ferrite and is also effective in increasing hardenability [37].

## 4.1.2Micro structural characteristics

Optical and scanning electron micrograph of the as-received steel is shown in Fig. 4.1 which reveals that the steel contain fully ferritic matrix with polygonal grains. Optical microstructures have been taken in three orientations R-D and T-D, which are illustrated in Fig. 4.1.

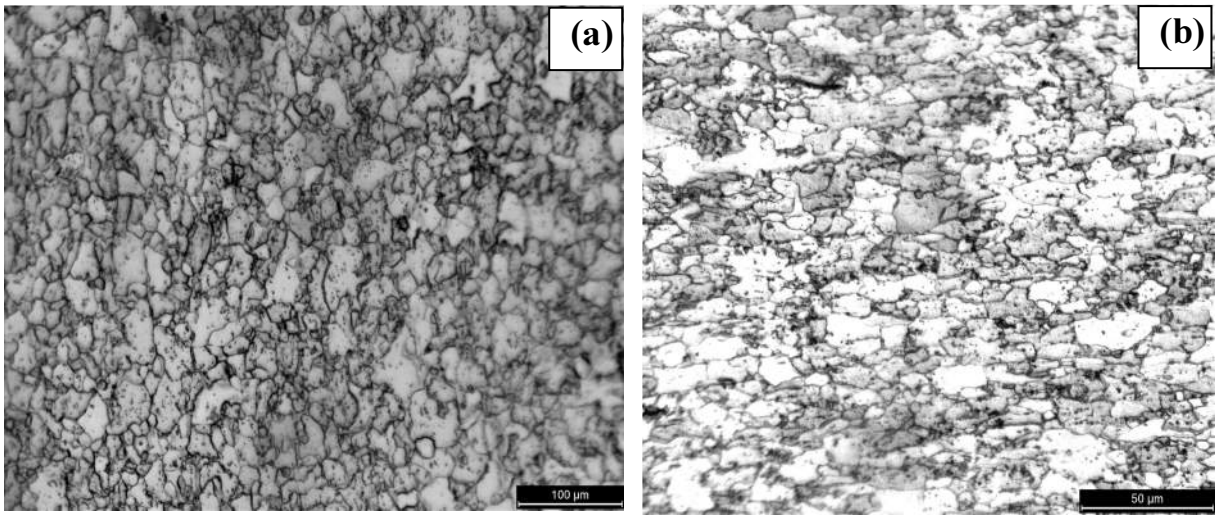


Fig. 4.1: Optical microstructures of the investigated steel in (a) Rolling direction, (b) transverse direction.

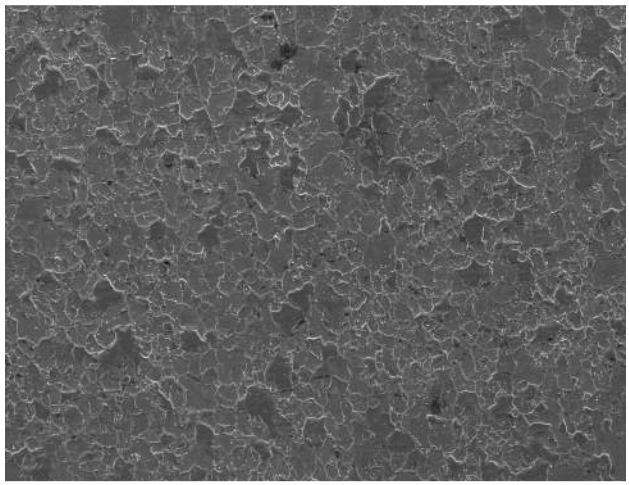

Fig. 4.2: Scanning electron micrograph of as received sample in rolling direction

Figure 4.2 is representing of typical scanning micrograph in rolling direction this figure it reveals fully ferrtic microstructure of investigated steel

.

### 4.1.3 Grain size measurements

The average grain size of the CMn440 steel was determined by the linear intercept method according to ASTM standard E-112 [38]. Linear intercepts are drawn on typical microstructure of higher magnification. For the calculation of grain size at least 10 good images were chosen. A grid of 10 horizontal lines was imposed on all these micrographs. The effective line lengths were calculated as per this micron marker of the image. Then all the intersections of the grid lines with grain boundary counted properly and grain sizes are estimated. In this method, the estimated average grain size is 17±1.70 μm. As can be seen from the adjoining plot in Fig. 4.3, the grain size distribution is quite homogeneous in nature.

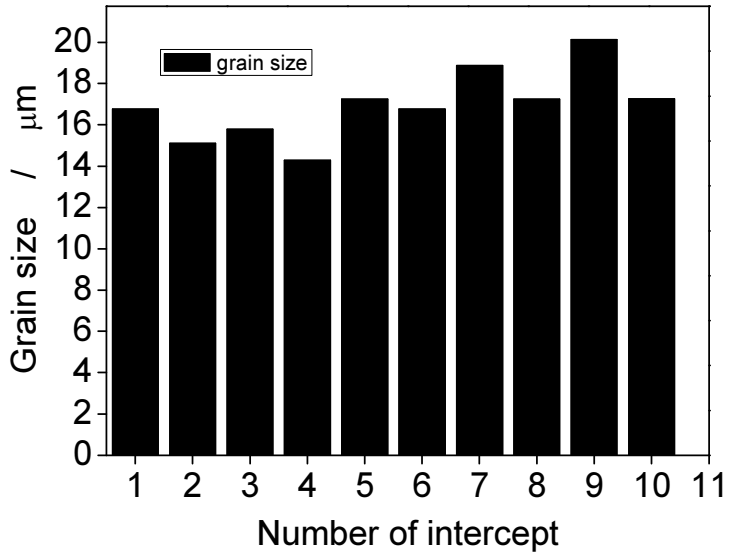


Fig 4.3: Typical grain size distribution for a particular micrograph of the investigated CMn440 steel.

### 4.1.4 Hardness

Hardness of the investigated CMn440 steel samples have been measured in different orientations by Vickers hardness tester. At least three readings have been taken at different positions for a comparative measurement. Care has been taken to keep at least 3 times

diagonal distance between two indentations. The dwelling time was 15 s, with applied load of 50 kgf. The results are tabulated in Table 4.2.

**Table.4.2 Hardness value of CMn440 steel**

| direction | Load (kgf) | Hardness (HV) |
|---|---|---|
| Rolling direction | 50 | 254 |
| Transverse direction | 50 | 251 |

## 4.2. Tensile behaviour of steel under varying strain rates

### 4.2.1Quasi-static and intermediate strain rates (Low strain rate tests)

It is well known that the quasi static range of strain rate is $10^{-5}$ to $10^{-1}$ $s^{-1}$and intermediate range of strain rate is $10^{-1}$ to 10 $s^{-1}$ [1]. The tensile tests were carried out under five different strain rates: 0.0001, 0.001, 0.01, 0.1, 1 $s^{-1}$. Three specimens were tested for each condition. All test results are shown in Table 4.1. The engineering stress vs. engineering strain curves of C-Mn440 steel are given in Fig. 4.4. It is observed that in line with natural expectation for most common metallic materials, the flow stress increases with increase in strain rate. The variations in the magnitudes of %uniform elongation (%UE) and %total elongation (%TE) are also shown in Fig. 4.5 which show that both %UE and %TE decrease steadily with increase in strain rate.

Table 4.1 Different strain rate test result

| Sample no. | Strain rate | UTS | YS | Uniform elongation |
|---|---|---|---|---|
| 1 | 0.0001 | 441 | 312 | 0.197 |
| 2 | 0.0001 | 471 | 315 | 0.196 |
| 3 | 0.0001 | 460 | 320 | 0.202 |
| 4 | 0.001 | 468 | 332 | 0.1857 |
| 5 | 0.001 | 465 | 325 | 0.1807 |
| 6 | 0.001 | 452 | 305 | 0.180 |
| 7 | 0.01 | 479 | 360 | 0.1699 |
| 8 | 0.01 | 483 | 347 | 0.1662 |
| 9 | 0.01 | 481 | 353 | 0.165 |
| 10 | 0.1 | 493 | 357 | 0.152 |
| 11 | 0.1 | 498 | 352 | 0.152 |
| 12 | 0.1 | 495 | 354 | 0.149 |
| 13 | 1 | 506 | 359 | 0.147 |
| 14 | 1 | 511 | 360 | 0.148 |
| 15 | 1 | 507 | 358 | 0.149 |

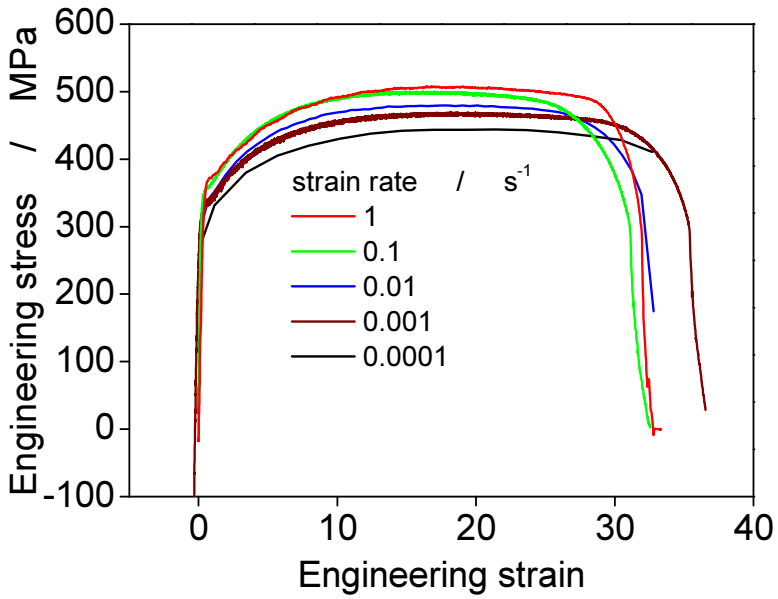


Fig.4.4 Engineering stress-engineering strain diagram

The engineering stress-strain diagrams have been analyzed to obtain yield strength (YS), ultimate tensile strength (UTS), percentage uniform elongation ($e_u$%) and percentage total elongation ($e_t$%).The yield strength has been determined using standard 0.2% offset method

for the specimens which do not show any yield point behavior; lower yield point has been taken as the yield stress where yield point phenomenon is observed [36].

The engineering stress at maximum load is designated as ultimate tensile strength (UTS). The magnitudes of uniform and total elongation values are estimated as the engineering strain corresponding to maximum load and that at break load respectively.

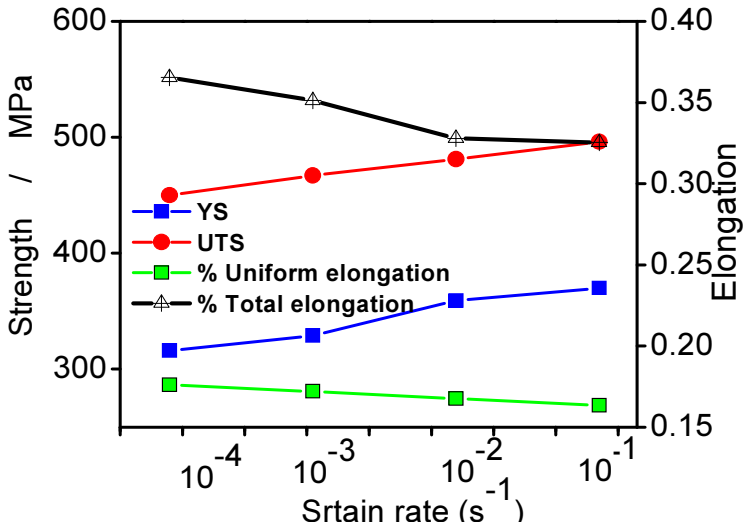


Fig4.5 Effect of strain rate on strength and ductile property

The nature of the stress- strain plots in Fig. 4.5 indicates that the ultimate tensile strength (UTS) and yield strength (YS) values increase with strain rate. In association to that, the uniform elongation and total elongation values decrease. The observed nature of increase in strength values is in line with natural expectation for most common metallic materials that the flow stress increases with increase in strain rate. The actual reason behind this kind of increase in strength values may be correlated with the variations of internal dislocation distribution of a material. It may be considered that dislocation pileup ahead of a barrier increases as the rate of deformation increases; following increase in the strain rates. If strain rates are increases the time taken in the deformation is less due to less time the dislocation move briskly and accumulated. For the accumulated dislocation high stress is required to

deform the material due to this UTS and YS increases. The above result obtained are in good agreement with the earlier reported results of Arpan et al. for the AISI304LN stainless steel [28,39].

As is discussed in the previous section, uniform elongation and total elongation of investigated steel decreases with increase the strain rate.

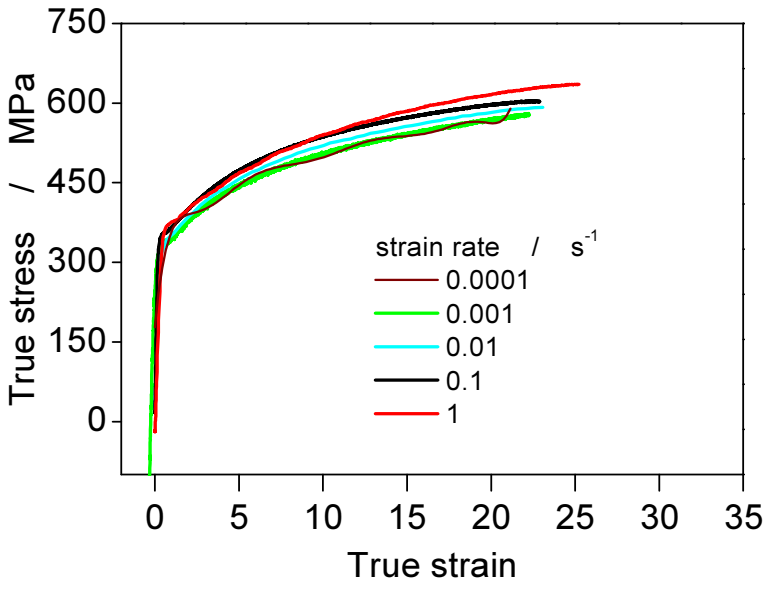


Fig 4.6 True stress-true strain diagram

Strain hardening exponent of the selected materials were calculated at each strain rates using the Hollomon equation,

$\sigma = K\varepsilon^{n}$ [1] (4.1)

The slope of the line obtained by linear regression of $\ln\sigma$ vs. $\ln\varepsilon_p$ values in the selected plastic strain range yields the value of strain hardening exponent. Figure 4.7 shows atypical $\log\sigma$ vs. $\log\varepsilon_p$ plot for calculation of strain hardening exponent.

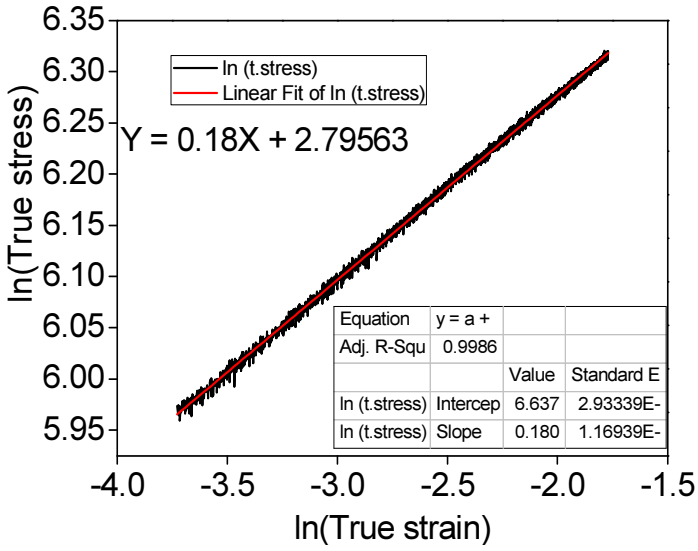


Fig 4.7: Typical lnσ vs. lnε plot obtained for estimation of strain hardening exponent.

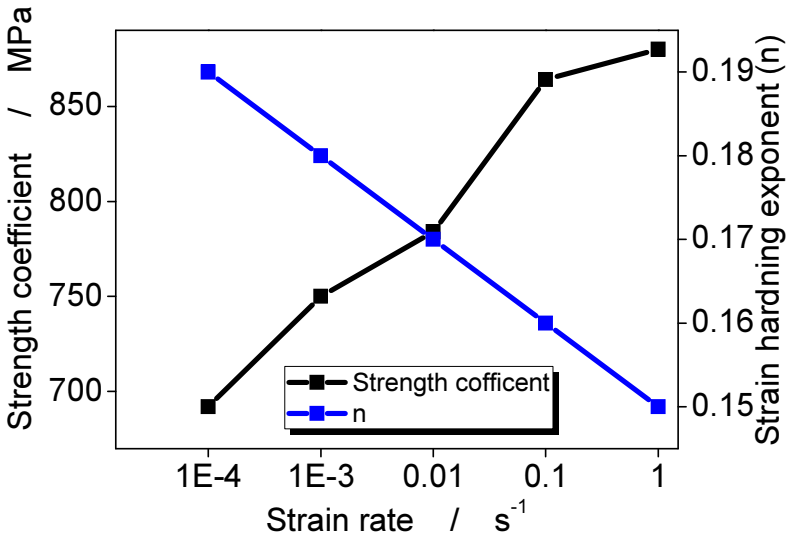


Fig .4.8: Effect of strain rate on strength coefficient and strain hardening exponent.

The variation in strain hardening exponent with strain rate of the selected materials in the investigated strain rate range is shown in Fig. 4.8. The strain hardening exponent is found to decrease as the strain rate increases from $10^{-4}$ to 1 $s^{-1}$. The above result obtained are in good agreement with the earlier reported results of arpan et. [28].

## 4.2.2 Fitting of flow curve

True stress (σ) and true strain (ε) values are calculated from engineering stress strain data using the relations:

$\sigma = s\,(1+e)$ (4.2)

$\varepsilon = \ln(e+1)$ (4.3)

Typical true stress-true strain plots calculated for the investigated steel at varying strain rate like $10^{-4}s^{-1}$, $10^{-3}\ s^{-1}$ ,$10^{-2}\ s^{-1}$,$10^{-1}s^{-1}$,$1\ s^{-1}$ are shown in Fig. 4.6.

The true stress-true strain curve is also known as flow curve. The tensile tests were carried out under five different strain rates: 0.0001, 0.001, 0.01, 0.1, $1\ s^{-1}$. Three specimens were tested for each condition. The true stress vs true strain curves of C-Mn440 steel are given in Fig. 4.6 It is observed that in line with natural expectation for most common metallic materials, the flow stress increases with increase in strain rate.

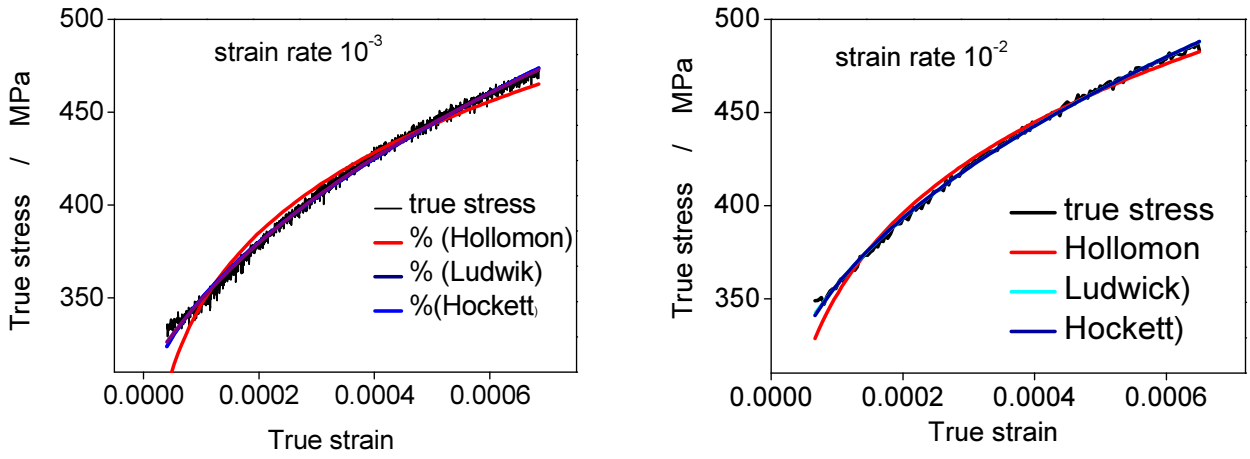

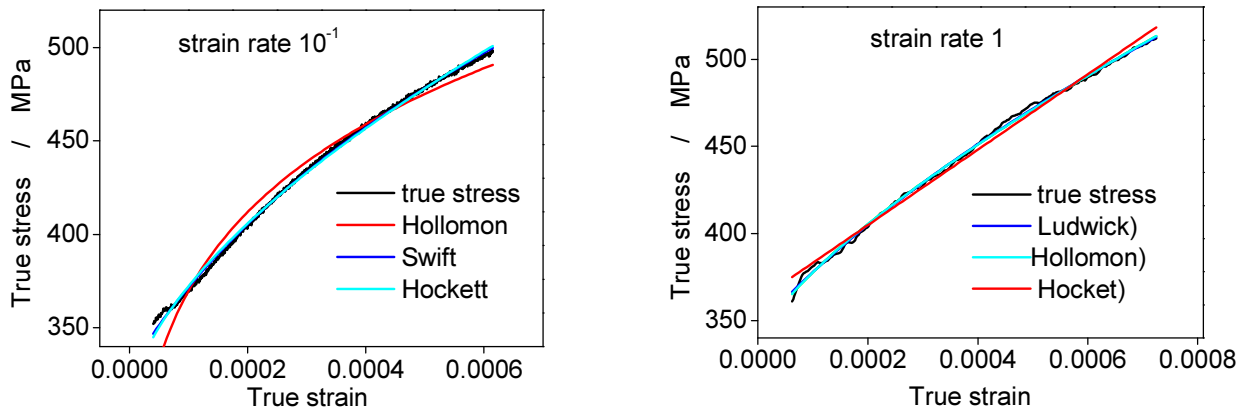


Fig.4.9 Flow curve fitting in plastic region at different strain rates.

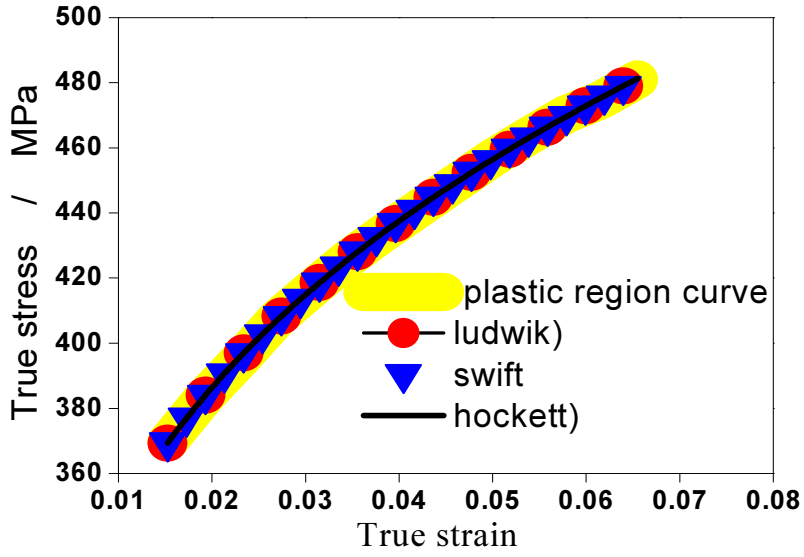


Fig. 4.10: Different consecutive relations for stress strain curve.

The flow curve of metals and alloys in the regime of uniform plastic deformation can be expressed by various empirical relationships proposed by Hollomon [$\sigma = K\epsilon^n$], Ludwick [$\sigma=C_1+C_2\epsilon^{C_3}$], Swift [$\sigma=C_1(C_2+\epsilon)^{C_3}$], Hockett [$\sigma=C_2-(C_2-C_1)exp(-C.\epsilon^{C_4})$] etc., where $K$ is the strength coefficient and $n$ is the strain hardening exponent. $C_1$, $C_2$, $C_3$, and $C_4$ are modelling parameters [40]. It can be seen from Fig. 4.9 Hollomon's model, all the above-mentioned model fit well to predict the plastic flow behaviour of the investigated steel.

### 4.2.3 Strain rate sensitivity:

Strain rate sensitivity values of the selected materials were calculated at five different true strain levels. These values selected by draw the line and corresponding each line select the true stress value from Figure 4.11(a). Figure 4.11(b) shows the variation of true stress with strain rates at true strains of 1%, 2%,3%,4% and 5%. True stress as expectedly increases with strain rate; the increase in true stress is found to be higher at lower strain levels than that at higher strain levels. The strain rate sensitivity at every true strain levels for the investigated steel are calculated and are shown in Fig. 4.11(c). Strain rate sensitivity is found to decrease with increasing strain levels. This causes decrease in strain hardening behavior and thus flow stress drops.

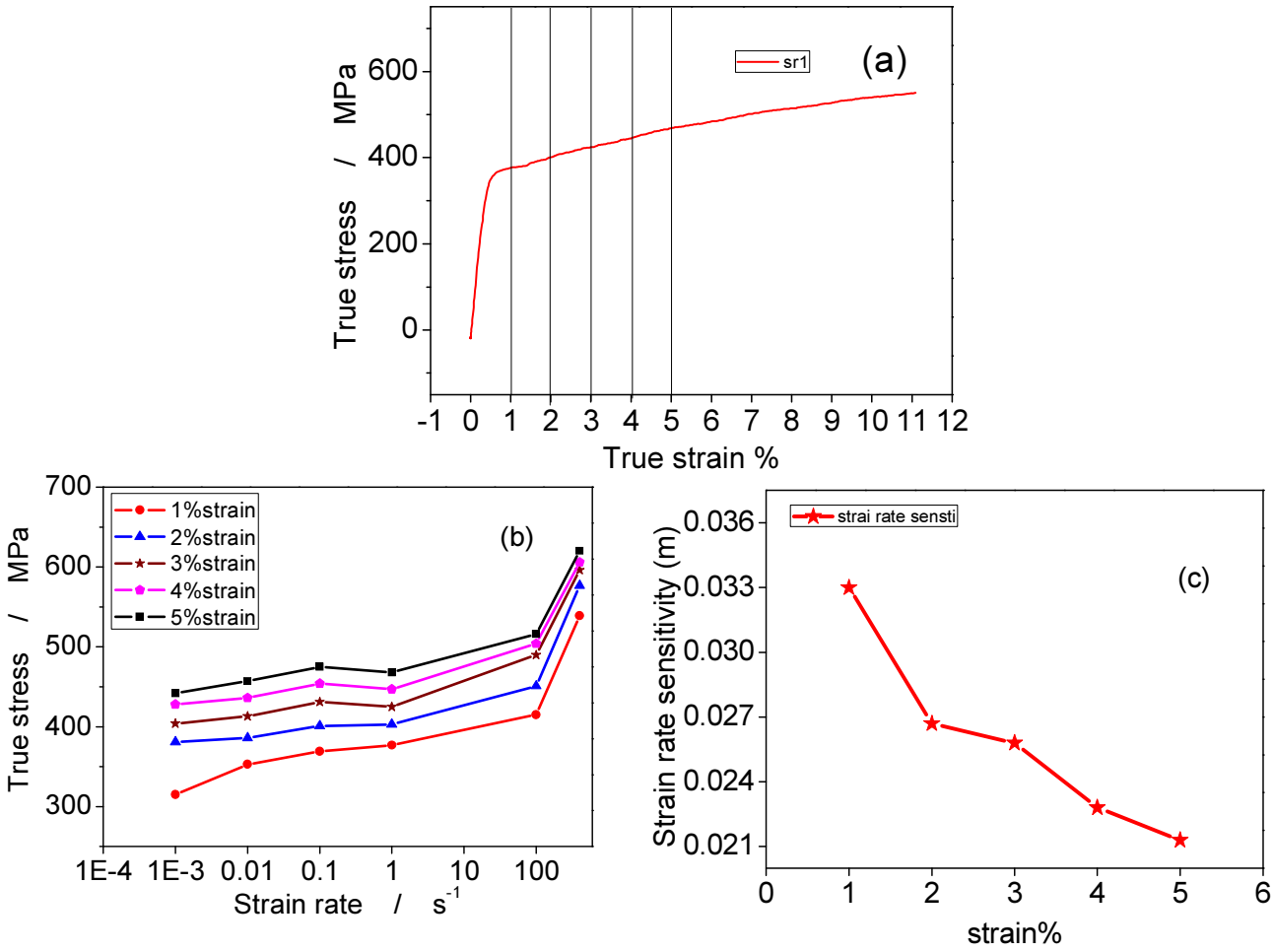


Fig 4.11 (a) Typical true stress-strain curve (b) variation of true stress at different true strain level with strain (c) variation of strain rate sensitivity with true strain for the investigated steel

### 4.2.4 High strain rate test

Figure 4.12shows the filtered engineering stress-strain curve obtained at high strain rates for the investigated steel. Fig 4.12 (a) consulted 100 and 400$s^{-1}$while Fig 4.12 (b) given for compression for allthe adopted strain rate. In both the cases, the yield strength and ultimate tensile strength values increase with increase in strain rate, To the contrary, percentage elongation is found to increase even the strength values increase. The increase in percentage elongation with strain rate when the applied strain rate is 100 $s^{-1}$ or above. The increase in percentage elongation may be attributed to thermal softening [17]. At such high speeds of deformation, thermal softening of a material occurs because of adiabatic heating which effects in increased percentage elongation of the material tested at high strain rate. Similar kind of behavior of increase in percentage elongation with increase in strain rate at $10^2$ $s^{-1}$ has been observed by many earlier investigators [39, 41 and 42] in case of TRIP, TWIP and DP steels respectively, where thermal softening stabilizes the retained austenite present in the microstructure which inhibits transformation of retained austenite to martensite during deformation. Increase in percentage elongation has also been observed by earlier reporters in interstitial free steels [43] when these are subjected to tensile loadings at order $10^2$ $s^{-1}$ of strain rate.

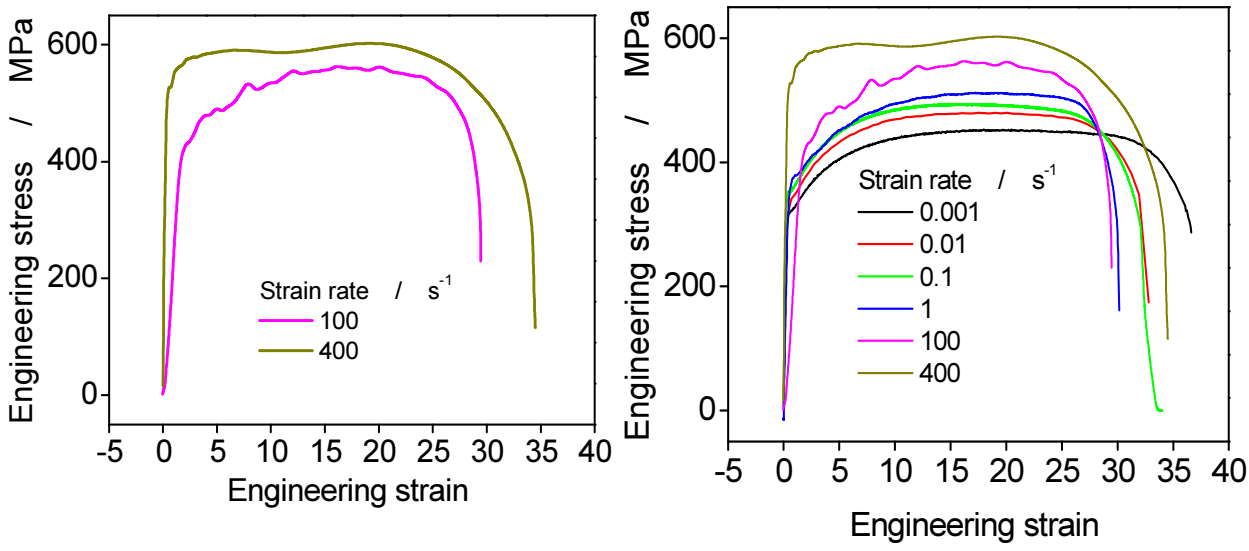


Fig 4.12. High strain rate tests .

## 4.3.Fractographic analysis

Typical fractographs are shown in figures 4.13(a) to 4.13 (e) for all the employed strain rates. As expected, all the fractographs exhibit typical ductile mode of fracture. Analyses of the fractographs obtained from the fracture surfaces of the five different samples reveal that there exists elongated dimples at the specimens belong to low strain rates, but at higher strain rates more amount of equi-axed dimples were found. It is observed that the mean dimple diameter increases with the strain rate, the minimum being at the lowest strain rate (0.0001 $s^{-1}$). It has been demonstrated elsewhere [28, 29] that deformation and fracture are influenced, to a large extent, by the same set of factors, and then the fracture surface keeps an imprint of the entire deformation process. Figure 8 clearly elucidate that the mean size of the dimples constituting the final fracture changes depending upon the strain rate. It was noted that, with decreasing strain rate, number of fine dimples becomes predominant, and with increasing strain rate, the fine dimples is gradually replaced by larger dimples.

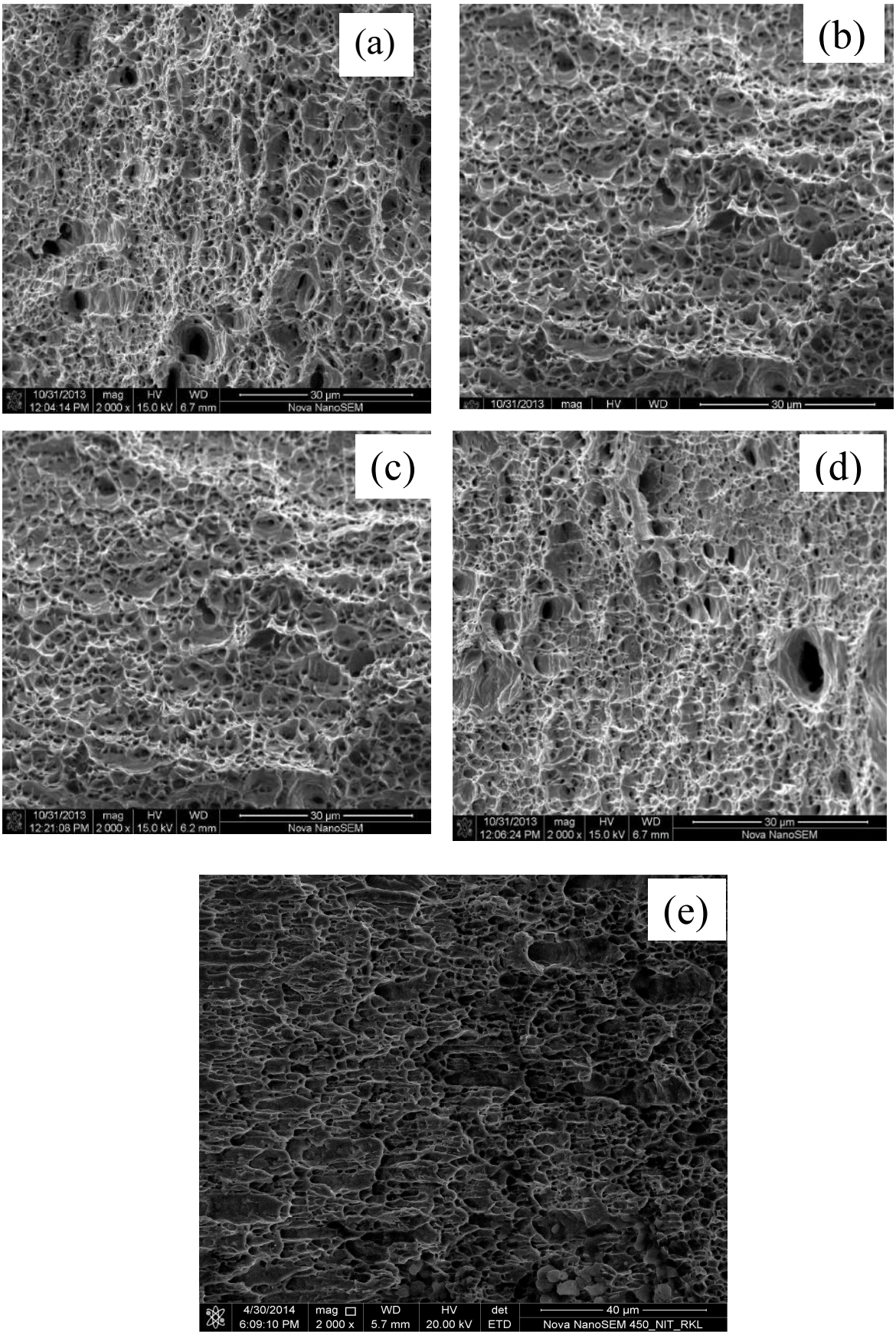


Fig 4.13 Fractographs of different strain rates sample (a) strain rate0.0001$s^{-1}$ (b)strain rate0.001$s^{-1}$ (c) strain rate 0.01$s^{-1}$ (d)strain rate 0.1 $s^{-1}$(e) strain rate 1$s^{-1}$

### 4.3.1 Effect of strain rate on ductile properties, mechanical properties and dimple density.

Figure 4.14 shows that the variation of strength properties with dimple diameter; Figure 4.15 shows the corresponding variation in ductility properties .it should be note that the dimple diameter decreases with decreases the strain rate, and dimple density increases with decrease the strain rate .this nature of variation of a dimple diameter with strain rate precisely similar to that of mechanical properties.

It is appears that there is a systematic correlation of the mechanical properties and the dimple diameter at ductile fracture with strain rate variation.

The important point to be notes is that an appropriate fractographic investigation can be used to make a reasonable estimate of the variation in the mechanical properties of deformation behaviour of material [27] The above result obtained are in good agreement with the earlier published report results of arpan et al[27].

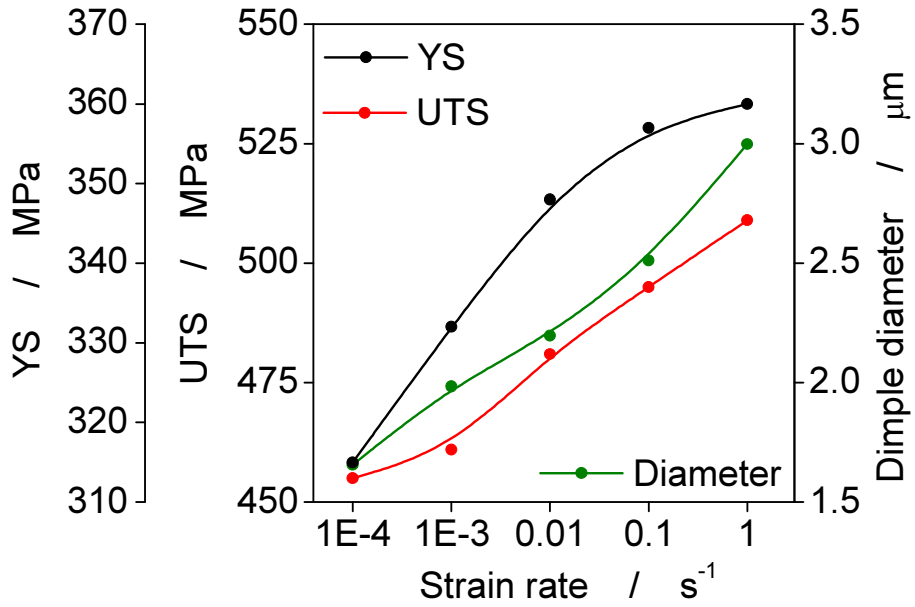


Fig 4.14 Effect of strain rate on strength and dimple diameter

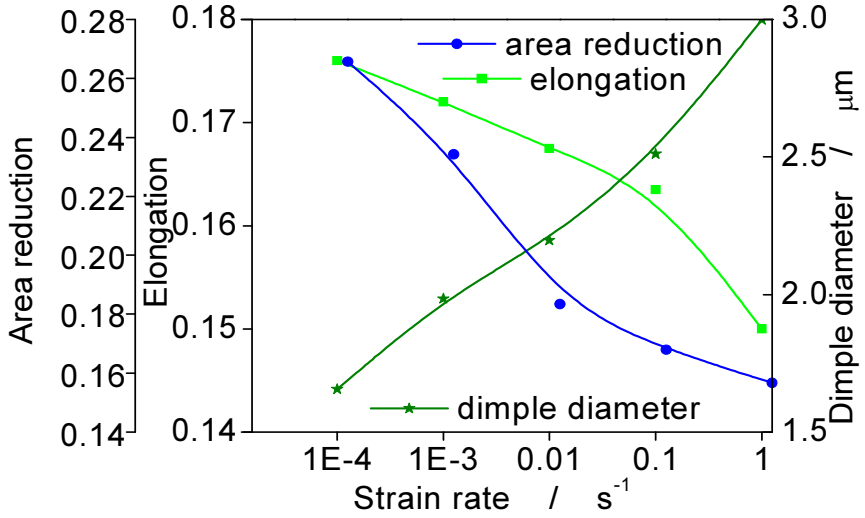


Fig 4.15 Effect of strain rate on ductility properties and dimple dia

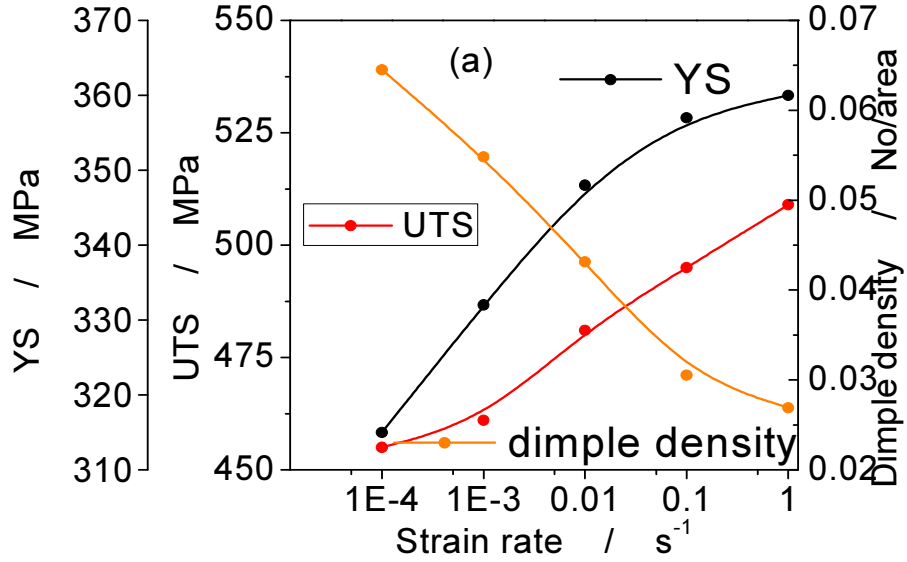


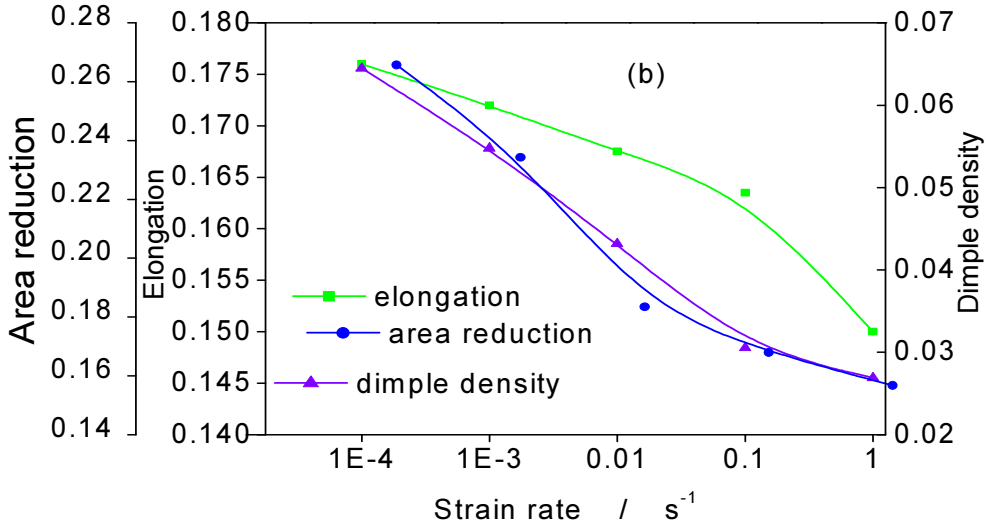


Fig .4.16 effect of strain rate (a) on strength and dimple density (b)on ductility properties and dimple density.

## 4.3.2 Occurrences and dimple diameter:

It is observed that the mean dimple diameter increases with the strain rate, the minimum being at the lowest strain rate (0.0001 $s^{-1}$). Minimum diameter is 0.29 mm at low strain rate. It is clearly found from figure. As well as increasing the strain rate the dimple size increases and dimple density decreases. The process was explained in section 2.9.1 in chapter 2. [28].

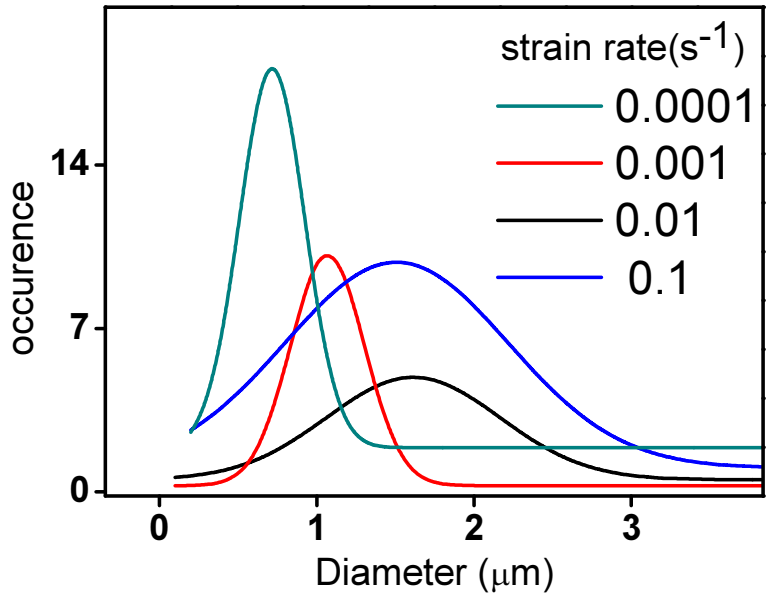


Fig. 4.17 Occurrences verses dimple diameter

## 4.4. Variation in the microstructure:

As the discuses section 4.1.3 the microstructure of investigated steel showing polygonal grain with grain size approximately 17 μm in rolling direction (RD).it was aim to study the variation in microstructure of the tensile tested specimens at a varying strain rate and the result of this analysis are plotted in Fig 4.18(a) and 4.18(b) respectively .for variation of grain size with true strain and that for grain aspect ratio.

Microstructure of collecting data in this Fig .4.18 the micrograph has been taken on polished and eatch surface away from the fracture end.

The result indicated that the grain size may vary from 14μm to 18 μm for the strain rate $10^{-4}$ $s^{-1}$ where as the grain size varies 20 μm to 32 μm at a strain rate 1 $s^{-1}$.it can be conclude from this result at low strain rate grain size dose not vary as such with true strain. To the contrary at strain rate 1 $s^{-1}$ the grain size increases about 75%at the maximum true strain level.

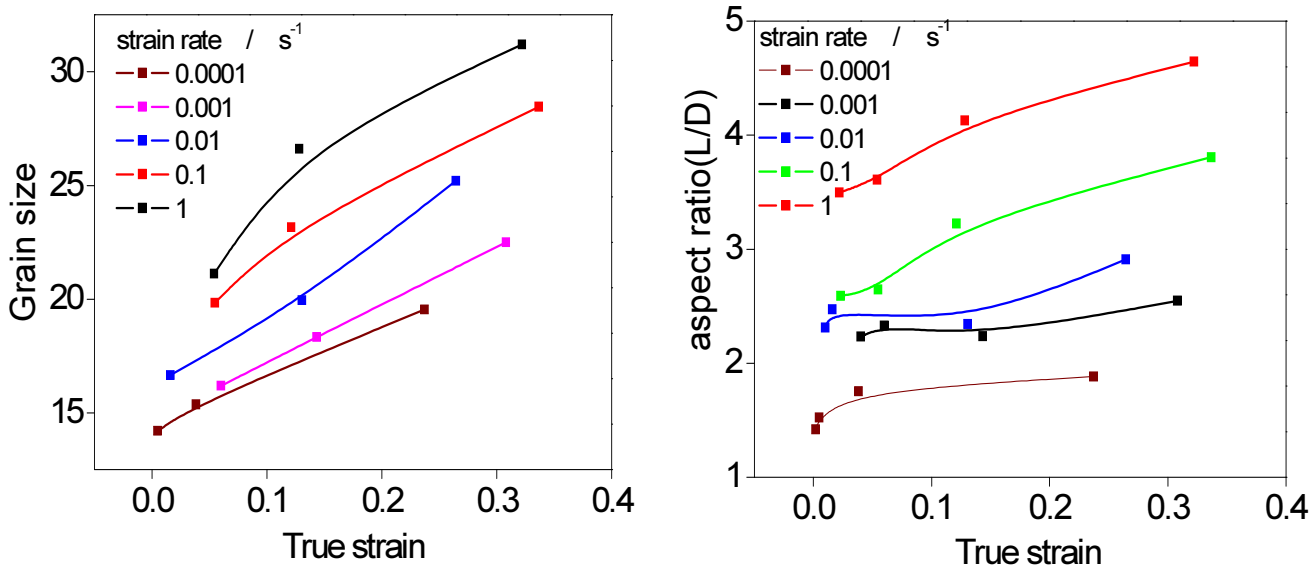


Fig 4.18 (a) Effect of strain rate on grain size with varying true strain (b) Effect of true strain on aspect ratio with varying strain rate

# 4.5. Damage accumulation:

The investigated steel is a automotive steel, hence the factor of safety is very important for that type of steels. In this connection, it is a-priori important to know the damage accumulation to this kind of steel. The micromechanism of ductile fracture is usually associated with formation of voids in the subsurface of the material. In view of formation of voids and its morphology during tensile loading under varying strain rates, thorough investigation was carried out on fractured tensile specimens at several levels of true strains, using optical microscopy. Typical void generation map is shown in Fig. 4.19. The voids as appeared in the micrograph were composed of elongated shapes. Fig. 4.21is represent the void density respectively with true strain of the fractured tensile specimens for all the investigated strain rates. It can be observed from Fig. 4.21that the rate of progress of the void population with strain is firstly low, and then increases briskly with high strains on approaching the fracture surfaces. For the same quantity of true strain or width strain, the void density fraction was observed to be higher for the high strain rate sample than for the low strain rate. Also, to arrive at the same amount of void density fraction, the higher strain rate specimen needs a lower amount of accumulated true strain than the lower strain rate. This is in agreement with some published reports on AISI 304LN stainless steel [29].

## 4.5.1 Void density and true strain variation:

The micromechanism of ductile fracture is usually associated with formation of voids in the subsurface of the material. In view of formation of voids and its morphology during tensile loading under varying strain rates, thorough investigation was carried out on fractured tensile specimens at several levels of true strains, using optical microscopy. Typical void generation map is shown in Fig. 4.19. The voids as appeared in the micrograph were composed of elongated shapes. Fig. 4.21 represents the void density respectively with true strain of the

fractured tensile specimens for all the investigated strain rates. It can be observed from Fig.4.21 that the rate of development of the void population with strain is initially low, and then increases rapidly with high strains on approaching the fracture surfaces. For the same amount of true strain, the void density fraction was found to be higher for the high strain rate specimen than for the low strain rate. Also, to reach the same amount of void density fraction, the higher strain rate specimen needs a lower amount of accumulated true strain than the lower strain rate. This is in accordance with some published reports on AISI 304LN stainless steel [28] state of stress, voids grow, coalesce and finally form the continued fracture surfaces with dimples. The dimples show the confirmation of the beginning points at the particles. Inclusions and secondary phase partial play an important role in this failure process in many materials, either they are present in a relatively small quantity [29].

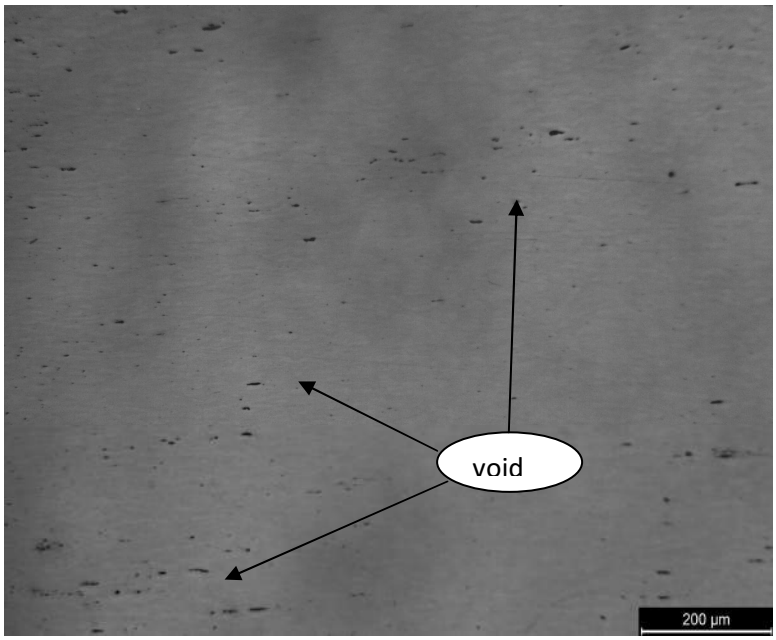


Fig..4.19 Optical micrograph showing presence of voids at sub-surface of fractured tensile specimen tested at strain rate $0.1s^{-1}$.

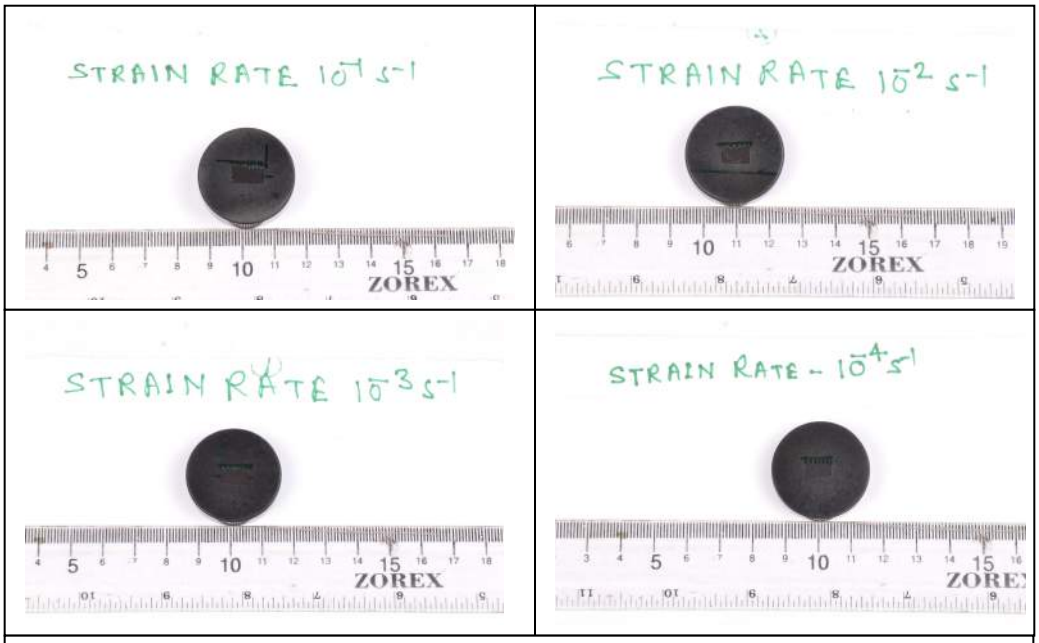


Fig 4.20 Deformed mounted sample at different strain rates.

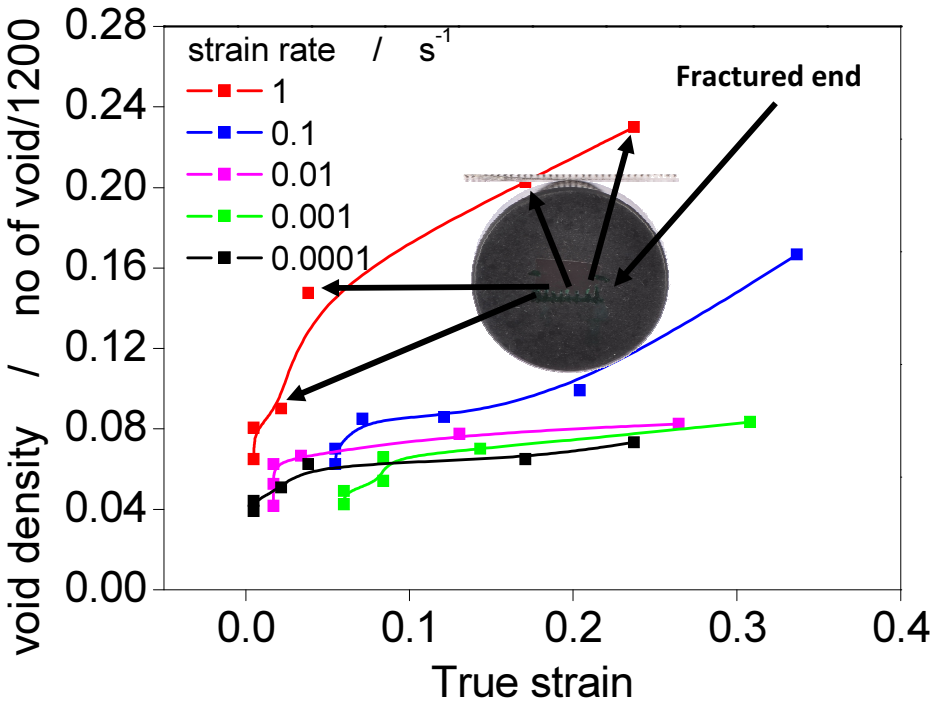


Fig.4.21. Variation of void density with true strain.

## 4.5.2Void count at tip at different true strain :

Void counting has been don as transverse section mounted fractured specimen following method describe in section2.9 in chapter.2.The calculation of void at tip position at different strain rate is varying with increasing strain rate .if the strain rate is increases the void count is increases at tip position. it is clearly shows in the figure at high strain rate $10^{-1}$ and 1 $s^{-1}$ the void count is very high in compare to low strain rate .the void count is 88 at very low strain rate at 0.0001 $s^{-1}$and at 0.001 $s^{-1}$ the void count is 92 and at strain rate 0.01 $s^{-1}$ void count is 100 and at high strain rate the void count is increase abruptly. At strain rate $10^{-1}$ $s^{-1}$ the void count at tip is 200 and void count at strain rate 1 $s^{-1}$ is 276.

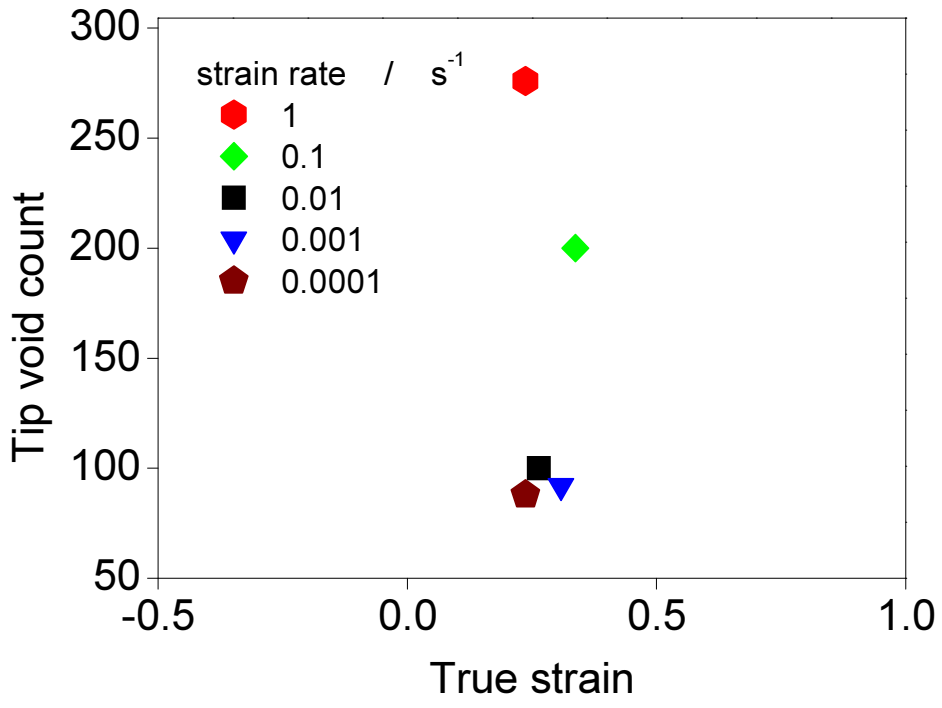


Fig 4.22. Void count at varying strain rate at tip

## 4.5.3Void aspect ratio:

Void aspect ratio is an increase with strain rate at the low strain rate the value of aspect ratio is low. With the variation of strain rate the void size was increases due to this the aspect ratio varies .it is investigated in the C-Mn440 steel the similar phenomena is occur.

At high strain rate the voids are elongated at the near to the fracture surface or at high true strain value due to this the void aspect ratio increases at high strain rate. The void are normally generate from the where the inclusions are present.

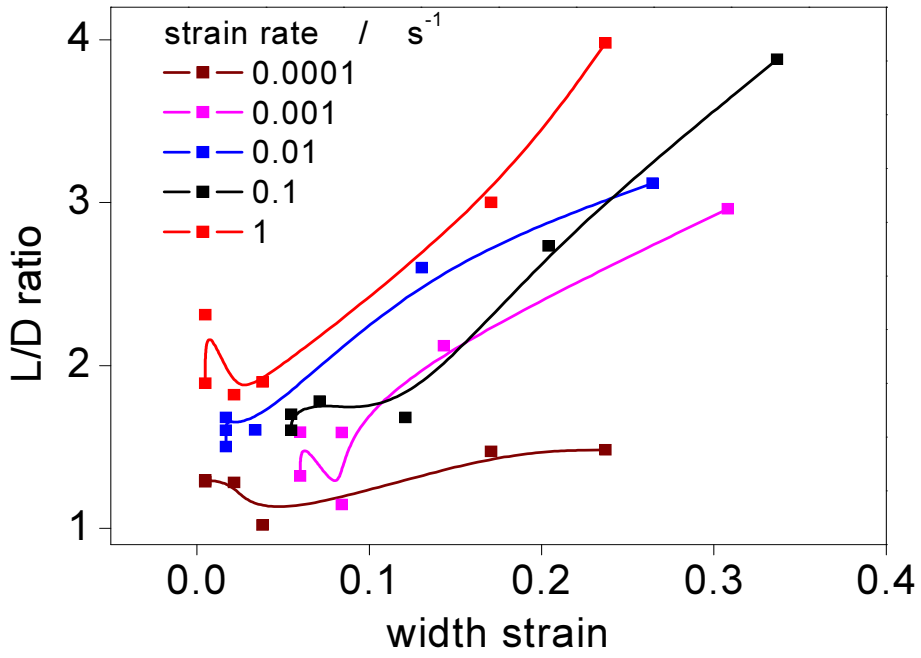


Fig 4.23 .Void aspect ratio with variation of strain rate.

## 4.6.X-ray analysis

Dislocation density of all the deformed specimen have been calculated using equation 2.1,2.2,2.3 of the section 2.11.1 in chapter 2. For this calculation we needed to know about the variation of ΔK vs $KC^{1/2}$ this of the modified Williamson–Hall equation .typical graph given in figure for this condition this condition .the dislocation density can be calculated by

$\rho=2m^2/\pi M^2b^2$ this equation.

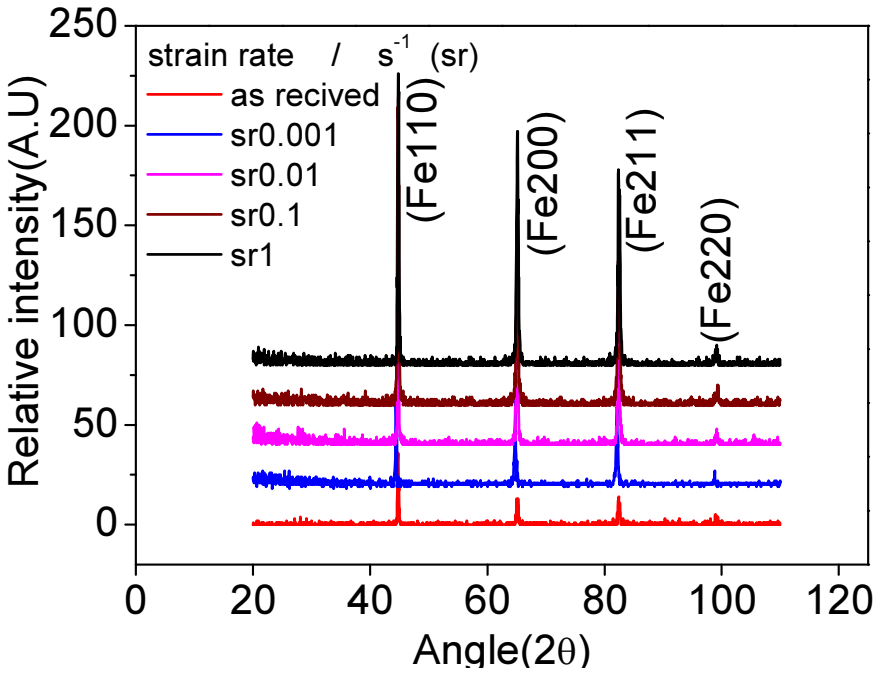


Fig .4.24 Relative intensity verses angle at varying strain rates

### 4.6.1Calculation of dislocation density

$$\rho = \frac{2m^2}{\pi M^2 b^2}$$

Where ρ =average dislocation density

M=2 is used for all the steel

b = magnitude of the Burgers vector

with the help ΔK vs. $K^2$ C plot find the value of m, where m is the slope of the linear fit of the data points.

Now here m=0.0041 and b=4.96405, M=2 (for steel)

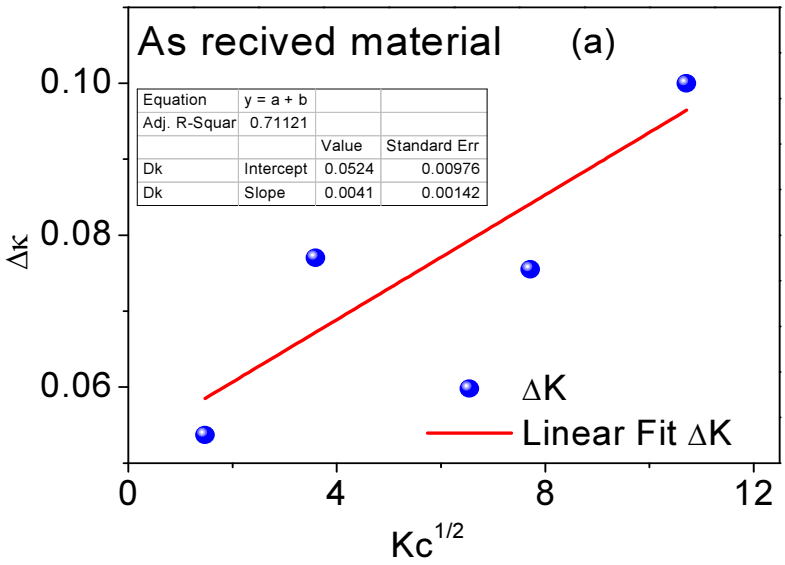


$\rho=2*(0.004)^2/\pi*4*(4.96405*10^{-10})^2$

**$\rho = 1.085717 \text{ X } 10^{13}$** (as received material)

m=0.00412 for strain rate $0.001s^{-1}$

$\rho=2*(0.00412)^2/\pi*4*(4.96405*10^{-10})^2$

**$\rho = 1.096717 \text{ X } 10^{13}$** (strain rate $0.001s^{-1}$)

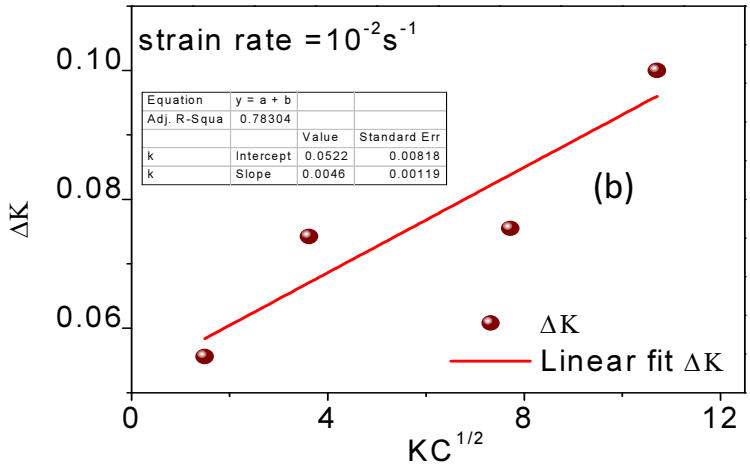


m=0.00462 for strain rate 0.001$s^{-1}$

$\rho=2*(0.0046)^2/\pi*4*(4.96405*10^{-10})^2$

**$\rho = 1.36717 \text{ X } 10^{13}$** (strain rate 0.01$s^{-1}$)

-

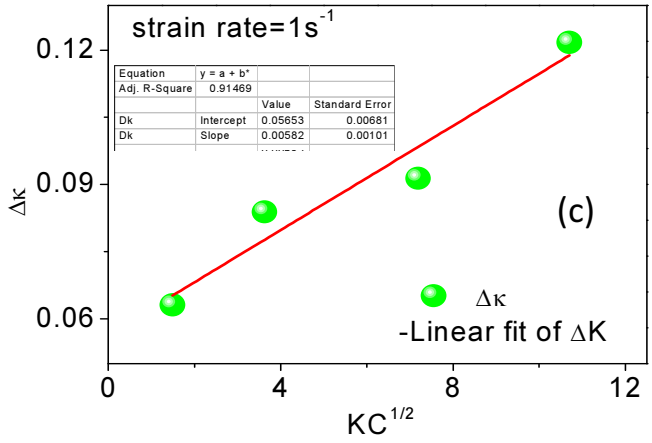


Fig.4.25 Peak broadening analysis using the modified Williamson hall plot (a) as received material (b) at strain rate 0.01 $s^{-1}$ (c) at strain rate 1 $s^{-1}$

m=0.0051 for strain rate 0.001$s^{-1}$

$\rho=2*(0.0051)^2/\pi*4*(4.96405*10^{-10})^2$

**$\rho = 1.6797 \text{ X } 10^{13}$** (strain rate 0.01$s^{-1}$)

m=0.00582 for strain rate $1s^{-1}$

$\rho=2*(0.00582)^2/\pi*4*(4.96405*10^{-10})^2$

**$\rho = 2.1877 \text{ X } 10^{13}$** (strain rate $1s^{-1}$)

**Table4.4 Effect of strain rate on dislocation density**

| **Strain rate $s^{-1}$** | **Dislocation density** |
|---|---|
| As received material | $\rho = 1.085717 \text{ X } 10^{13}$ |
| 0.001 | $\rho = 1.096717 \text{ X } 10^{13}$ |
| 0.01 | $\rho = 1.36717 \text{ X } 10^{13}$ |
| 0.1 | $\rho = 1.6797 \text{ X } 10^{13}$ |
| 1 | $\rho = 2.1877 \text{ X } 10^{13}$ |

From above result it has been conclude that the dislocation density is increases with strain rate. Initial stage of strain rates the dislocation increase slowly and later stage is drastically increased

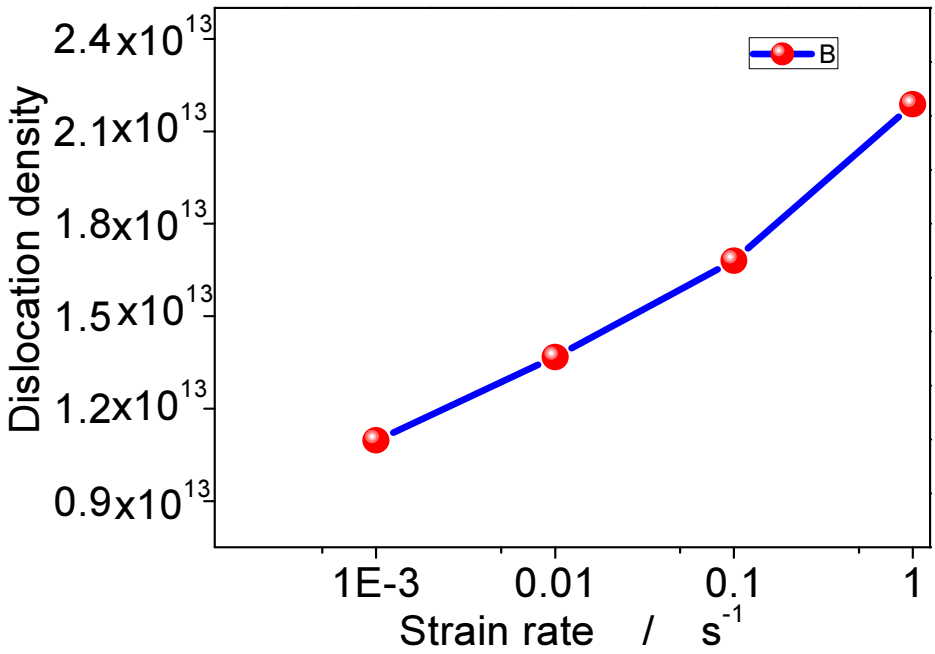


Fig 4.26 Effect of strain rate on dislocation density

# CHAPTER-5

# CONCLUSIONS AND SCOPE FOR FUTURE WORK

# Conclusions:

The obtained results and their pertinent analyses related to different strain rate deformation behavior of CMn440 steel and its associated variations in property assist to infer

- Both yield strength (YS) and ultimate tensile strength (UTS) increase when experiments are conducted under increasing strain rate. On the other hand, % uniform elongation and % total elongation decrease with increasing strain rate, as expected. It has been observed that parameters like strain hardening exponent ($n$), strength coefficient ($K$) increase with strain rate; these have been obtained from the plastic region of the true stress – true strain curve using Hollomon equation. Empirical equations by Hollomon, Ludwik, and Hockett fit well to the entire plastic regime of the true stress – true strain curve as well.
- Fractographic investigations reveal typical ductile fracture characteristics associated with dimples of bimodal size distribution. A comparative assessment of dimple geometry on the fracture surfaces clearly reveals that with the increase in strain rate, average dimple diameter increases and dimple density decreases and *vice versa*.
- The void accumulation (i.e., void density) in the subsurface of the material (near the fracture surface) increases with the increase in true strain for all strain rates. At the initial stage of strain, void density increases slowly and at the later stage, void density increases rapidly
- Void density is dependent on the strain rate at it increases with increasing the strain rates.

## Scope for future research:

1. The damage accumulation has been assessed up to strain rate $1s^{-1}$ in the current investigation hence this fact for high strain rate (100,400 $s^{-1}$) can be investigated.
2. TEM study for all the deformed specimen must revelled or must generate various information which has not be addressed in this investigation hence this study can be done.
3. Compare of dislocation density value obtained from TEM and XRD can be done.
4. Fracture mechanism investigation and study for higher strain rate sample.

# REFERENCES

[1] Dieter G.E., (1988) “Mechanical Metallurgy”, McGraw-Hill Book Company,.

[2] Scott C., Allain S., Faral M. and Guelton N. (2006), “The Development of new Fe-Mn-C austenitic steel for automotive application” .publication on line by Cambridge university,06 293-302.

[3] Gurson.L A., Trans.ASME(1977), J. Eng. Mat. Tech. 992–15.

[4] Wilsius J., Imad A., Naitabdelaziz M., Measmacque G., Eripret C. (1999), Fat. Fract. Eng. Mat. Str. 23 105–112.

[5] Krivoglaz A M.., (1996),Theory of X-ray and “Thermal Neutron Scattering by Real Crystals”, Plenum Press, New York,

[6] Faraji G., Mashhadi M.M., .Bushroa R A., .Babaei A (2013),Mater.Sci.Eng.A563 193–198.

[7] Shintani T., Murata Y. (2011),ActaMater.59 4314–4322.

[8] Gubicza J., Szepvolgyi J., Mohai I., Zsoldos L., Ungar T. (2000),Mater.Sci.Eng.A280 263–269.

[9] Hordon J M.., Averbach .L B. (1961),ActaMetall.9247–249.

[10] Bodin A. (2001) , Materials Characterization 47 187– 193

[11] ASM Handbook (2000), Vol. 8, Mechanical Testing and Evaluation, US, ASM International, Metals Park, OH, The Materials Information Society, 9th Edition, pp. 939–1270.

[12] Odeshi, A.G., -ameeri Al, S. and Bassim, M.N. (2005), "Effect of high strain rate on plastic deformation of a low alloy steel subjected to ballistic impact", Journal of Materials Processing Technology, Vol. 162–163, pp. 385–391.

[13] Marchand, A. and Duffy, J. (1988), "An experimental study of the formation process of adiabatic shear bands in a structural steel", Journal of Mechanical Physics and Solids, Vol. 36, No. 3, pp. 251-283.

[14] Shastry, C. G., Parameswaran, P., Mathew, M.D., Rao, K. Bhanu, Sankara. and Mannan, S.L. (2007), "The effect of strain rate and temperature on the elevated temperature tensile flow behavior of service-exposed 2.25Cr-1Mo steel", Materials Science and Engineering A, Vol. 465, pp. 109–115.

[15] Meyers M. C. and Wittman, C. L. (1990), "Effect of Metallurgical Parameters on Shear Band Formation in Low-Carbon Steels", Metallurgical Transactions A, Vol. 21A, pp. 3153-3164.

[16] Zener, C. and Hollomon, J. H. (1944), "Effect of Strain Rate Upon Plastic Flow of Steel", Journal of Applied Physics, Vol. 15, pp. 22-32.

[17] Timothy, S. P. (1987), "The Structure of Adiabatic Shear Bands in Metals: A Critical Review", Acta Metallurgica, Vol. 35, No. 2, pp. 301-326.

[18] Huh, H., Kima, S., Songa, J. and Lim, J. (2008), "Dynamic tensile characteristics of TRIP type and DP-type steel sheets for an auto-body", International Journal of Mechanical Sciences, . 918–93.

[19] Wei, X., Fu, R. and Li, L. (2007), "Tensile deformation behavior of cold-rolled TRIPaided steels over large range of strain rates, Materials Science and Engineering A", Vol. 465, pp. 260–266.

[20] Lee, W.-S.; Lin, C.F. (2002), "Comparative study of the impact response and microstructure of 304L stainless steel with and without pre-strain. Metall". Mater. Trans.A,33App. 2801-2810.

[21] Yoshizawa, M.; Ohsawa, H(1997), "Evaluation of strain rate sensitivity in superplastic compressive deformation". J. Mater. Process. Technol., 68 pp. 206-214.

[22] Wagoner H R., Wang M N., (1983), "Operant strain-rate sensitivity during tensile necking.Metall". Trans. A, 14A, Nov. pp. 2395-2406.

[23] Miura K., TakagS. i, Furukimi O., Obara, T. Tanimura S. (1996), "Dynamic deformation behavior of steel sheet for automobile". SAE 960019 .

[24] Yan B., Urban D., Characterization of fatigue and crash performance of new generation high strength steels for automotive applications. DE-FC07-97ID13554, AISI/DOE (2003).

[25] Wilson D.W, Strain rate sensitivity and effects of strain rate in sheet forming. Met. Technol.(1980) pp. 282-292.

[26] Das A., Das S .K., Sivaprasad S. and Tarafder S., "Fracture-property correlation in copper-strengthened high-strength low-alloy steel", Scripta Mater.,vol. 59 (7),pp. 681 – 683, 2008.

[27] Das A., Tarafder S., "Geometry of dimples and its correlation with mechanical properties in austenitic stainless steel" Scripta Mater. 59 (2008) 1014–1017.,

[28] Das A. and Tarafder S.,"Experimental investigation on martensitic transformation and fracture morphologies of austenitic stainless steel", Int. J. Plast, vol. 25 (11), pp. 2222–2247, 2009.

[29] Das A. "Martensite – Void Interaction", Scripta Mater., vol. 68, pp. 514 – 517, 2013.

[30] KishoR., Sahu L., .Dutta K and Mondal A.K., " Assessment of dislocation density in asymmetrically cyclic loaded non conventional stainless steel using X-ray diffraction profile analysis" Mater.Sci.Eng.A598(2014) 299-303.

[31] .Ungár T, BorbélA. y,Appl.Phys.Lett.69(1996)3173–3175.

[32] Ungár T., Gubicza J., Hanak P. and Alexandrav I.;"Densities and character of dislocations and size-distribution of sub grains in deformed metals by X-ray diffraction profile analysis" Mater.Sci.Eng.A309–310 (2001)14–22.

[33] Ribarik G., Ungár T., "Characterization of the microstructure in random and textured polycrystals and single crystals by diffraction line profile analysis" Mater.Sci.Eng.A528 (2010) 112–121.

[34] Renzetti R.A., .Sandim H.R.Z, Bolmaro R.E., Suzuki Moslang, P.A.,A. "X-ray evaluation of dislocation density in ODS-Eurofer steel"Mater.Sci.Eng. A534(2012)142–146.

[35] E112, "Standard test methods for determining grain size", Annual book of ASTM standards, West Conshohocken, PA, 2003.

[36] ASTM E8M "Standard Test Methods for Tension Testing of Metallic Materials [Metric]," ASTM, International, West Conshohocken, PA, USA, 2004.

[37] ASM handbook volume 1 properties and selection iron steel and high performance alloy1990

[38] R.G.Xiong, R.Y.Fu, Y.Su, Q.Li and L. Li, "Tensile properties of TWIP steel at high strain rate", J. Iron Steel Res. Int., vol. 16, pp. 81 – 86, 2009.

[39] Potrick larour,ing,Walfgang Black,Dierk Raabe "strain rate sensitivity of automotive sheet steel :influence of plastic strain ,strain rate, temperature microstructure bake hardening and pre strain",ISBN 978-3-8322-9149-2 ,2010.

[40] Rong T.,Lin L., Cooman B.C.D., chen W.Xi-, and Peng S., (2006), "Effect of Temperature and Strain Rate on Dynamic Properties of Low Silicon TRIP Steel", Journalof Iron and Steel Research, International, Vol. 13(3), pp. 51-56

[41] Da-zhao Li., Hui Ying, Wei., Chun-yue, Lid., Li-feng, Hod., Dong-Ieng, Lid. and Xianzhe,In. (2010), "Effects of High Strain Rate on Properties and Microstructure Evolution of TWIP Steel Subjected to Impact Loading", Journal of Iron and Steel Research, International. Vol. 17(6), pp. 67-73.

[42] Kuroda.M., Uenish.A., Yoshida H., and Igarashi A., (2006), 'Ductility of interstitial-free steel under high strain rate tension: Experiments and macroscopic modeling with a physically-based consideration", International Journal of Solids and Structures, Vol. 43, pp. 4465-4483.

# Publications

[1] **A. k Mishra**, A. Das,S.Shivaprasad K. Dutta, "Deformation behavior of C-Mn440 steel under varying strain rates" published in the proceedings (ISBN978-81-928552-1-9 pp 315-319) of the International Conference on Emerging Materials and processes-2014, Bhubaneswar,India.

[2] L. Sahu, **A. K. Mishra** and K. Dutta, Ratcheting behaviour of a non-conventional stainless steel and associated microstructural variations, Journal of Materials Engineering and Performance, **paper accepted for publication.**

# National and International conferences

[1] Paper presentation on "International Conference on Emerging Materials and Processes - 2014". **(ICEMP 2014) CSIR-IMMT,Bhubaneswar**.

[2] Paper presented on 3rd National Conference on Processing and Characterization of Materials **NCPM 2013** at National Institute of Technology Rourkela.